

José Miguel Branco Marques

Battery Management System (BMS) for Lithium-Ion Batteries

Master Dissertation

September 2014



UNIVERSIDADE DE COIMBRA



UNIVERSITY OF COIMBRA
FACULTY OF SCIENCES AND TECHNOLOGY
ENERGY FOR SUSTAINABILITY INITIATIVE

Battery Management System (BMS) for Lithium-Ion Batteries

José Miguel Branco Marques

Coimbra, 2014

Battery Management System (BMS) for Lithium-Ion Batteries

Submitted in partial fulfillment of the requirements for the degree of
Master of Science in Energy for Sustainability
Faculty of Sciences and Technology, University of Coimbra

Submitted by:

José Miguel Branco Marques

Under supervision of:

Prof. Dr. Aníbal Traça de Almeida

Jury:

Prof. Dr. Manuel Carlos Gameiro da Silva

Prof. Dr. Pedro Manuel Soares Moura

Prof. Dr. Aníbal Traça de Almeida

September 2014

“People who are really serious about software should make their own hardware.”

-Alan Kay.

Acknowledgements

This dissertation would not be the same without the generosity and contribution of a large number of people.

I would like to thank my supervisor, Professor Dr. Aníbal Traça de Almeida, for its trust and for the possibility of developing this work on the challenging field of Battery Management Systems for Electric Vehicles.

I am also very grateful to all my colleagues that assisted me in different ways. I appreciate very much their suggestions and the time they spent to support me, helping to achieve this important milestone. Special Thanks to Fábio Faria, Marco Silva, João Sousa, Luis Garrote and André Gonçalves that worked close to me and helped to shape the final product.

I thank ISR and Professor Dr. Urbano Nunes for providing the excellent conditions and resources that allowed me to accomplish this dissertation. This work has been supported by project Grant "PROJECTO B: Diagnosis and Assisted Mobility for People with Special Needs" (QREN-MAIS Centro: CENTRO-07-ST24-FEDER-002028).

I am very grateful to all my friends and to my family for their continuous support. Finally, last but not least, I would like to express my greatest gratitude to my girlfriend, Adélia, from who I was absent for longer times than I wished. Her support and understanding was essential, especially in the most difficult moments.

Resumo

O desenvolvimento de Veículos Eléctricos (EV) é na actualidade alvo dos fabricantes de automóveis e pode ser considerado como uma solução imediata para um sistema de transporte rodoviário sustentável, pela sua contribuição na redução da emissão de gases geradores do efeito de estufa.

Os EVs têm como componente principal o sistema de armazenamento de energia. Este sistema envolve para além da bateria, todos os sistemas de gestão e monitorização da mesma, vulgarmente denominados pela sigla BMS do termo inglês “Battery Management System”. As baterias usadas em EVs têm exigências elevadas em termos de segurança, densidade de potência (aceleração), densidade de energia (autonomia), elevada eficiência, ciclos de descarga profundos e reduzidas taxas de auto-descarga entre outras. De entre as várias composições químicas disponíveis para a construção de baterias, as baseadas em Lítio-Ferro-Fosfato (LiFePO₄), Lítio-Ítrio-Ferro-Fosfato (LiYFePO₄) ou Lítio-Manganésio (LiMn₂O₄) são as mais seguras e duradouras e como tal são estudadas no ISR-UC.

Os sistemas de gestão e monitorização de energia dedicados a EVs utilizam métodos de estimação do estado de carga proprietários, não permitindo a sua utilização de forma simples nem a sua melhoria. Por este motivo foi desenvolvido no ISR uma nova solução aberta e flexível que permite estudar novos algoritmos de estimação do estado de carga.

Durante esta dissertação, instalou-se e testou-se um BMS comercial na bateria de Iões de Lítio que alimenta uma das plataformas disponíveis no ISR-UC, o ISRobotCar. Uma segunda plataforma, que foi re-instrumentada no decorrer deste projecto, também necessitou de substituição das suas baterias de chumbo originais por se encontrarem em fim de vida.

Devido às limitações encontradas em BMSs comerciais, desenvolveu-se de raiz um novo BMS, designado nesta dissertação por ISR-BMS, que instrumenta uma nova bateria de LiYFePO₄.

O estado de carga das baterias é uma informação fundamental para os utilizadores de EVs. No entanto o estado de carga não é uma grandeza mensurável e apresenta uma grande dependência da temperatura e das condições de operação da bateria. Existem várias técnicas utilizadas para a estimação do estado de carga, que requerem a utilização de modelos das células com diferentes complexidades. Para o ISR-BMS adoptou-se o modelo do circuito eléctrico equivalente e modelizou-se uma célula de Iões de Lítio de 90Ah, baseado em testes laboratoriais a diferentes temperaturas e ciclos de descarga.

Após a instalação do ISR-BMS na plataforma, efectuaram-se testes de condução real com vista à validação das medições efectuadas e recolhidas do ISR-BMS.

Palavras-chave: Sistema de Gestão de Baterias, Baterias de Iões de Lítio, Modelização de Células de Iões de Lítio, Estimação do Estado de Carga (SOC).

Abstract

The Electric Vehicle (EV) is already on the roadmap of every important car manufacturer and is seen as the solution to a more sustainable transport system, contributing to a reduction of the Greenhouse Gas Emissions.

The Energy Storage System (ESS) is a key component for EVs. This includes the battery and all the management and monitoring systems that compose the Battery Management System (BMS). Those batteries have very demanding requirements regarding safety, power density (acceleration), energy density (autonomy), high efficiency, deep discharge cycles or low self-discharge rates to name a few. From the available chemistries for the construction of EV batteries the Lithium-Iron-Phosphate (LiFePO₄), Lithium-Yttrium-Iron-Phosphate (LiY-FePO₄) or Lithium-Manganate (LiMn₂O₄) are the most safe and long lasting and because of that they are studied at the ISR-UC.

The energy monitoring and management systems for EVs use proprietary State of Charge (SOC) algorithms that do not allow their easy use or improvement. For this reason was developed at the ISR-UC a new BMS with an open and flexible architecture allowing the implementation of new SOC estimation algorithms, the ISR-BMS.

During this dissertation, a commercial BMS was installed and tested on a Lithium-Ion battery pack that powers one of the electric platforms available at the ISR-UC. A new platform was completely re-instrumented during the course of this project and required a new ESS to replace their original lead acid batteries, which became end of life.

The SOC of the battery is a vital information to the EV user. It can be displayed as the percentage of full charge capacity that is still available from the battery or be used to estimate the vehicle range based on additional information from previous driving cycles. However, it can not be measured directly from the battery and have a strong dependence with the temperature and the operating conditions.

Several SOC estimation techniques are mentioned on the literature, that require cell models with different complexity and computer process requirements. In this work an Equivalent Electrical Circuit (EEC) model was adopted, with its parameters estimated based on experimental data collected through cell testing at different temperatures and charge/discharge current profiles.

After installation of the ISR-BMS on the platform, on-road drive tests were performed to acquire relevant information and validate the accuracy of collected measurements.

Key words: Battery Management Systems (BMS), Lithium-Ion Batteries, Cell Modeling, State of Charge (SOC).

Contents

Acknowledgements	i
Resumo	ii
Abstract	iv
List of Figures	xi
List of Tables	xiii
Nomenclature	xv
1 Introduction	1
1.1 Motivation and context	1
1.2 Objectives	2
1.3 Implementations and key contributions	2
1.4 Structure of the dissertation	3
2 State of the Art	5
2.1 Battery Introduction	5
2.2 Batteries for Electric Vehicles	7
2.2.1 Battery Requirements	7
2.2.2 Lithium-Ion Battery Chemistries	8
2.2.3 Battery Safety	11
2.2.4 Life Span of Lithium-Ion Batteries	12
2.2.5 Aging Of Lithium-Ion Batteries	14
2.2.6 Performance of Lithium-Ion batteries	15
2.2.6.1 Efficiency	15
2.2.6.2 Capacity Change with Temperature and Discharge Rate	15
2.3 Battery Management Systems	16
2.3.1 Battery Modeling	19
2.3.2 Cell Balancing	20
3 ISR-Battery Management System	23
3.1 Preliminary Work	23
3.1.1 Energy Storage System selection for the new developed platform	26
3.2 BMS requirements	27

3.3	ISR-BMS Development	28
3.3.1	Hardware	28
3.3.1.1	The MAX14921 Analog Front End(AFE) Integrated Circuit . .	29
3.3.1.2	BMS Microcontroller	32
3.3.1.3	Current Sensor	32
3.3.1.4	Temperature Sensor	33
3.3.1.5	Communication Interface Hardware - USB	33
3.3.1.6	Communication Interface Hardware - CAN bus	33
3.3.2	Firmware	33
3.3.2.1	Real Time Operating System - FreeRTOS	33
3.3.2.2	Cells Voltage Measurement Procedure	34
3.3.2.3	Cell Balancing	36
3.3.2.4	Communication Protocol for BMS Parametrization and Data Logging	36
3.3.3	The BMS Graphical User Interface for PC	40
4	Battery Modeling	43
4.1	Modeling Method	43
4.2	Description of Tests Performed	45
4.2.1	Pre-conditioning	46
4.2.2	Characterization Test Setup	47
4.2.3	Characterization Tests	49
4.3	Cell Model Derivation	49
5	BMS Experimental Results	53
5.1	Battery Pack Current Measurements	53
5.2	Cell Voltages Measurements	53
5.3	Battery Balancing	55
5.4	ISR-BMS Benchmarking	58
6	Conclusion and future work	59
6.1	Conclusion	59
6.2	Future work	59
	Bibliography	61
	A BMS Schematics	66
	B Firmware File Structure	69
	C BMS-ISR Graphical User Interface (GUI)	70

D Winston Battery Datasheet

71

List of Figures

2.1	Individual Cell and 8-Cell battery pack.	6
2.2	Lithium-ion internal representation.	6
2.3	Energy&power demands in batteries for different vehicle applications.[Rosenkranz et al.,]	8
2.4	Typical energy density for batteries and liquid fuels. [Tie and Tan, 2013]	9
2.5	Comparing power and energy density of different chemistries. [CARB, 2007] . .	9
2.6	Tradeoffs among the five principal Lithium-Ion battery technologies. [BCG, 2010]	10
2.7	Schematic drawing of shapes and components of several Lithium-ion battery configurations: a – Cylindrical; b – Coin; c – Prismatic; d – Thin and flat. [Tarascon and Armand, 2001]	11
2.8	Lithium Battery from Boeing Dreamliner Airplane safety failure.	12
2.9	Safety failure related mechanisms on cell level. [Electropaedia, a]	13
2.10	Illustration of a battery with 80% DOD/SOC window. [Energy, 2012]	14
2.11	Capacity variation with temperature. [Electropaedia, b]	15
2.12	Capacity reduction at different temperatures and discharge rates. [Electropaedia, b]	16
2.13	Cell balancing topologies.	21
3.1	ISR-UC Electric Vehicle	23
3.2	Lithium-Ion battery pack acquired to the company Autosil S.A. (72V, 3kWh, 24 modules in series with 4 parallel cells each - 4P24S).	24
3.3	ORION BMS.	24
3.4	TC Charger.	24
3.5	Battery test setup.	25
3.6	Discharge logging of Autosil battery pack constant current discharge (15A). . . .	25
3.7	Energy Storage System of the newly developed platform	27
3.8	ISR-BMS Architecture	28
3.9	Hardware development workflow.	29
3.10	Battery voltages with different cathode chemistries. [Electronicdesign, 2012] . .	29
3.11	ISR-BMS Architecture.	31
3.12	Circuit Board bottom side derived from Eagle Layout Software.	31
3.13	HTFS200 - Hall-effect current sensor from LEM manufacturer.	32
3.14	MAX14921 cell voltages measurement procedure flowchart.	35
3.15	MAX14921 SPI Control of cells voltage readout.	36
3.16	Balancing flowchart.	37

3.17	Smartphone display of ISR-BMS voltages and temperatures.	39
3.18	ISR-BMS GUI parametrization menu.	40
3.19	ISR-BMS GUI live cell voltages plot.	41
4.1	EEC model adopted for ISR-BMS	44
4.2	Voltage plot of first pre-conditioning cycle.	47
4.3	Cell characterization test setup.	48
4.4	Characterization cell box GUI.	49
4.5	Measured versus simulated data at 25 °C.	50
4.6	EEC estimated parameters.	50
5.1	Comparative current measurements of ISR-BMS and Fluke i310s current probe.	54
5.2	Voltage measurements logged on the PC during a real road drive.	54
5.3	BMS debugging after installation.	55
5.4	Cell voltages during charge at 10A constant current.	56
5.5	Combined information of ISR-BMS, GPS and encoders from the electric platform during a real road drive.	57
5.6	Benchmarking the ISR-BMS with other commercial BMSs.	58
A.1	BMS-ISR Schematics 1/2	67
A.2	BMS-ISR Schematics 2/2	68
B.1	Firmware file structure (by Doxygen)	69
C.1	ISR-BMS GUI.	70
D.1	Winston battery LYP90AHA.	72

List of Tables

2.1	Comparative analysis of commercially available BMS ICs.	18
2.2	Advantages and limitations of existing Lithium-Ion modeling methods. [Antaloae et al., 2012]	19
2.3	Comparison of different cell balancing methods. [Rahimi-eichi, 2013]	22
3.1	Cost/performance comparison of possible alternative BMS architectures.	31
3.2	ISR-BMS Communication Protocol	38
3.3	OBDII commands implemented on ISR-BMS.	39
4.1	Overview of Applicable International Standards for Lithium-Ion cells or batteries	44
4.2	LFP090AHA cell specifications.	46
4.3	Test Setup Features	48

Nomenclature

API	Application Programming Interface
BEV	Battery Electric Vehicle
BMS	Battery Management System
C-rate	Discharge current required to fully discharge the battery in one hour
CAN	Controller Area Network
CC/CV	Constant Current/Constant Voltage
EEC	Equivalent Electrical Circuit
EKF	Extended Kalman Filter
ESS	Energy Storage System
EV	Electric Vehicle
FET	Field Effect Transistor
GHG	Greenhouse Gas
GUI	Graphical User Interface
HEV	Hibrid Electric Vehicle
I2C	Inter-Integrated Circuit
IC	Integrated Circuit
ICE	Internal Combustion Engine
ISR	Institute of Systems and Robotics
ISR-BSM	New BMS developed for ISRobotCar
OBDII	On Board Diagnostic System
OEM	Original Equipment Manufacturer
PID	Proportional-Integral-Derivative
SAR	Successive Approximation Register

SOC	State Of Charge
SOH	State of Health
SOL	State of Life
SPI	Serial Peripheral Interface

Chapter 1

Introduction

This chapter presents the work developed under this Master project. It starts with the motivations and context of the developed work. The main concepts involved are introduced as well as the main objectives and key contributions. Finally the whole document structure is presented.

1.1 Motivation and context

It is now unanimous that it is necessary to act fast to revert the negative effects of climate changes caused by massive Greenhouse Gas (GHG) emissions and CO₂ in particular. The road traffic is heavily dependent on fossil fuels and therefore it is one of the major contributors for those emissions. On the other hand more and more people are living in urban areas with negative impact on the air quality. The Electric Vehicle (EV) is seen as a potential solution to minimize those effects due to its high efficiency and zero emissions during the use phase.

Further-more, EVs can actively interact with the electrical grid since they can be used as an energy bank for energy storage from renewable power sources, known as vehicle to grid interaction. Another interesting application consist in the use of EVs as controllable loads in demand response programs.

However, there are still some restrictions related to autonomy and price, that limit its wide acceptance. The main reason for this, relies on the batteries, the most bulky and expensive component of an EV.

The EV is already on the roadmap of every important car manufacturer. It is expected a continuous evolution on the different fields that will conduct to lighter materials (like composite materials), batteries with higher energy density and longer life span, faster and more efficient charging. The price is expected to decrease as well, promoting the adoption of efficient and sustainable electric mobility solutions. The EV is seen as the solution to a more sustainable transport system that can contribute to a reduction of GHGs emissions and the import of crude oil, due to a much higher efficiency, from 28-30% of an Internal Combustion Engine (ICE) vehicle to 74-85% of an EV, and zero tailpipe emissions [Faria et al., 2013]. In Portugal, even with the actual energy mix, EVs can deliver an overall reduction of GHG emissions.

During the course of this work, two electric platforms were equipped with Lithium-Ion battery packs. For one a full battery pack and a commercial BMS were installed. After testing the system some flexibility was missing to implement different balancing algorithms. It was

also impossible to change the simple State Of Charge (SOC) estimation procedure based on coulomb counting and voltage drift that needs to be fully programmable by the user.

1.2 Objectives

The objectives of this work were defined as follows:

1. Design a new BMS platform based on available dedicated integrated circuits and micro-controllers targeting fast sampling, high accuracy, low consumption and low cost;
2. Build an open system that allows the implementation of different charging and balancing algorithms, and that is able to be used with different battery models;
3. Install a fully functional prototype on a ISR EV;
4. Develop the required experimental testing to validate the concept;
5. Benchmark existing commercial BMSs in comparison with the ISR-BMS.

1.3 Implementations and key contributions

The main implementations and contributions can be summarized as follows:

1. Installation of a commercial BMS on a 72V, 40Ah, 3kWh Lithium-Ion battery pack in collaboration with the colleague Marco Silva;
2. Development of a new BMS architecture, including hardware, software and Graphical User Interface (GUI).
3. Instrumentation with the new BMS architecture of a new battery pack (72V, 90Ah, 6.5kWh) to power a new electric platform;
4. Individual cells were tested in laboratory under controlled temperature and charge/discharge conditions;
5. The parameters of an Equivalent Electrical Circuit (EEC) were estimated based on the experimental data fitting using a Matlab model [Huria et al., 2010] and estimation software;
6. The BMS current measurement accuracy was verified against a commercial Fluke current probe (Model i310s) on a road test drive.

1.4 Structure of the dissertation

On Chapter 1, the work developed under this Master Dissertation is presented as well as the motivations and context of the developed work. The main concepts involved are introduced, as well as main objectives and key contributions. On Chapter 2 the key components of a Battery Management System are explored. The latest developments on the field of batteries, BMS and cell modeling are presented as well. On Chapter 3 the architecture of the ISR-BMS and the choices undertaken are justified. An overview of the whole design process is presented, as well as the key features of the developed hardware and software. Chapter 4, explains the modeling process of a Lithium-Ion cell and discusses the model features and the model parameters estimation based on experimental data collected in the laboratory. A cell characterization setup, built for this purpose, is also briefly described. On Chapter 5, several experimental tests made with the EV after the ISR-BMS installation are described. The measurements taken by the ISR-BMS are verified. Its on-line performance as well as its ability to safely charge and balance the battery pack are also presented. Finally, on Chapter 7, the conclusions and some topics for future work are presented.

Chapter 2

State of the Art

On this chapter the key components of a Battery Management System are explored. The latest developments on the field of batteries, BMSs and cell modeling are presented.

Batteries play an important role on EVs. They are the sole power supply of the whole system. EVs demand the use of high performance batteries that can deliver the required power and energy and still weight as less as possible. Different battery technologies are available nowadays but only a few are suitable for automotive applications. Lithium-Ion based batteries are one of the most promising technologies. Battery systems require the use of a BMS that monitors their state and guarantees their operation within safe limits and optimizes the use of available capacity. Prior to discuss the BMS, the batteries are introduced and their key parameters are presented with special focus on the Lithium-Ion chemistry.

2.1 Battery Introduction

A battery is an electrochemical device that converts the chemical energy contained in its active materials directly into electrical energy. In automotive rechargeable systems the battery is recharged by the reversal of this process. While the term “battery” is often used, the basic electrochemical unit is the “cell”. A battery consists of one or more of these cells, connected in series or parallel, or both, depending on the desired output voltage and capacity. Figure 2.1 shows a single cell and a battery pack with 8 cells connected in series.

The cell consists of three major components (represented in Figure 2.2):

1. The anode or negative electrode - the reducing or fuel electrode - that releases electrons to the external circuit and is oxidized during the electrochemical reaction;
2. The cathode or positive electrode - the oxidizing electrode - that accepts electrons from the external circuit and is reduced during the electrochemical reaction;
3. The electrolyte - the ionic conductor - that provides the medium for transfer of charge, as ions, inside the cell between the anode and cathode. The electrolyte is typically a liquid, such as water or other solvents, with dissolved salts, acids, or alkalis to improve ionic conductivity. Some batteries use solid electrolytes, which are ionic conductors at the cell operating temperature.



Figure 2.1: Individual Cell and 8-Cell battery pack.

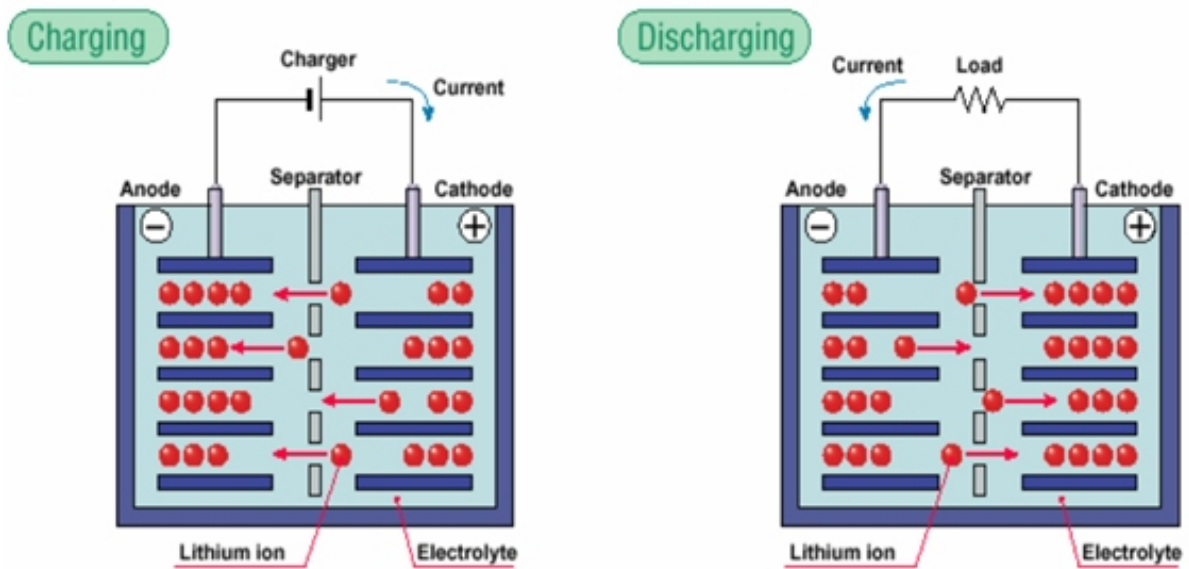


Figure 2.2: Lithium-ion internal representation.

2.2 Batteries for Electric Vehicles

EVs need a portable source of electrical energy. All this energy is previously stored on the Energy Storage System (ESS) that should match the energy requirements of the different car systems (traction, lighting, climate control) and guarantee a reasonable autonomy. With existing state-of-the-art technology, most of this energy is stored in batteries (sometimes complemented with super-capacitors or flywheels to improve response to peak demands).

2.2.1 Battery Requirements

EV batteries or traction batteries differ from the typical automotive battery in internal combustion engines. The latest are also known as SLI batteries (Starting, Lighting, Ignition) because they are used to power the start motor, the lights and the ignition system of a conventional car engine. Those are typically lead-acid type, and are made of six galvanic cells in series to provide a 12V system. They need to supply high current peaks for short time and they work mostly close to full charge capacity.

Usually the two battery types coexist on an EV with different functions. The traction batteries need to be designed to provide energy to the electric motor for long periods. They need as well to provide some peak power during fast acceleration.

EV Battery Operating Requirements:

- Large capacity batteries are required to achieve reasonable range. A typical EV uses around 100 to 150 Wh per kilometer depending on the terrain and the driving style.
- The battery must be capable of regular deep discharge (80% Depth of Discharge (DOD) or higher) operation;
- It is designed to maximize energy content and deliver full power even with deep discharge to ensure long range;
- A range of capacities will be required to satisfy the needs of different sized vehicles and different usage patterns;
- Must accept very high repetitive pulsed charging currents when regenerative braking is applied;
- Without regenerative braking, controlled charging conditions and lower charging rates are possible ;
- Routinely receives a full charge;
- Often also reaches nearly full discharge;
- Fuel-gauging warning near "empty" point;

- Needs a Battery Management System (BMS);
- Needs thermal management;
- Typical voltage $> 300\text{V}$;
- Typical capacity $> 20 - 60\text{kWh}$.

Typical energy and power requirements for different vehicle applications can be found in Figure 2.3.

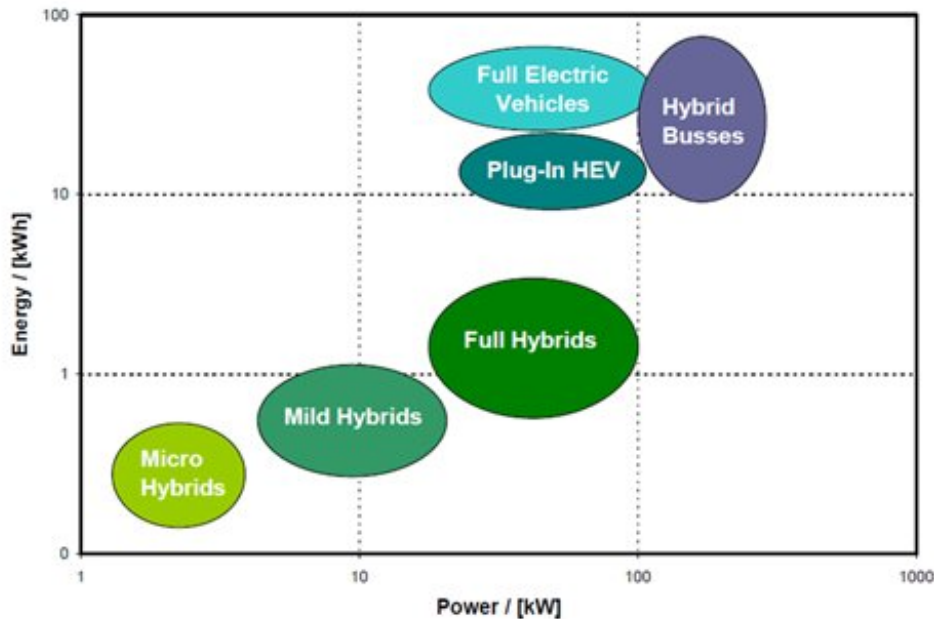


Figure 2.3: Energy&power demands in batteries for different vehicle applications.[Rosenkranz et al.,]

Batteries for EVs are characterized by their relatively high power-to-weight ratio, energy-to-weight ratio and energy density. Smaller, lighter batteries reduce the weight of the vehicle and improve its performance. Compared to liquid fuels, nowadays, battery technologies have much lower specific energy (Figure 2.4) and this often influences the maximum all-electric range of the vehicles.

In automotive battery applications, as can be seen in Figure 2.5, the primary trend is increasing energy density. This has favored a move towards Lithium-Ion chemistries, even though other chemistries can demonstrate greater longevity, and lower specific costs.

On this basis, the remainder of this section is focused on Lithium-Ion chemistries, their operation, potential and drawbacks.

2.2.2 Lithium-Ion Battery Chemistries

Lithium-Ion batteries comprise a family of battery chemistries that employ various combinations of anode and cathode materials. Each combination has distinct advantages and

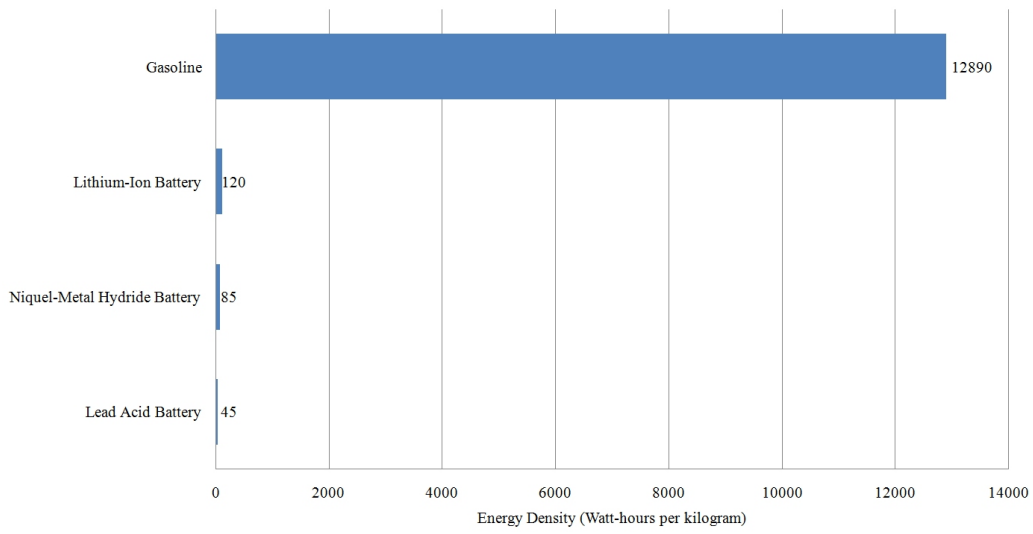


Figure 2.4: Typical energy density for batteries and liquid fuels. [Tie and Tan, 2013]

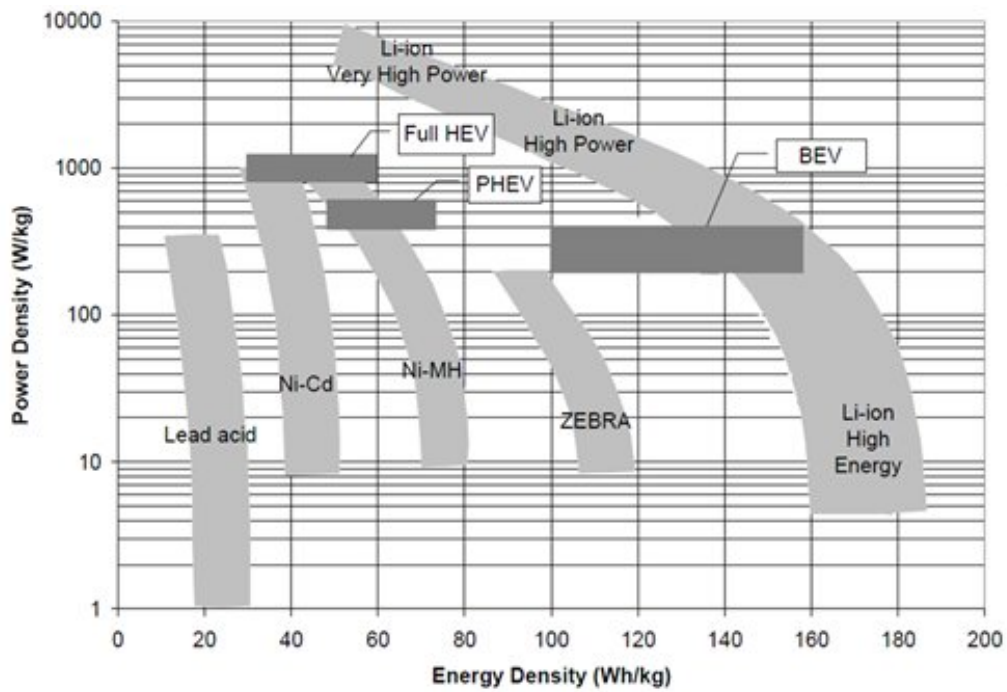


Figure 2.5: Comparing power and energy density of different chemistries. [CARB, 2007]

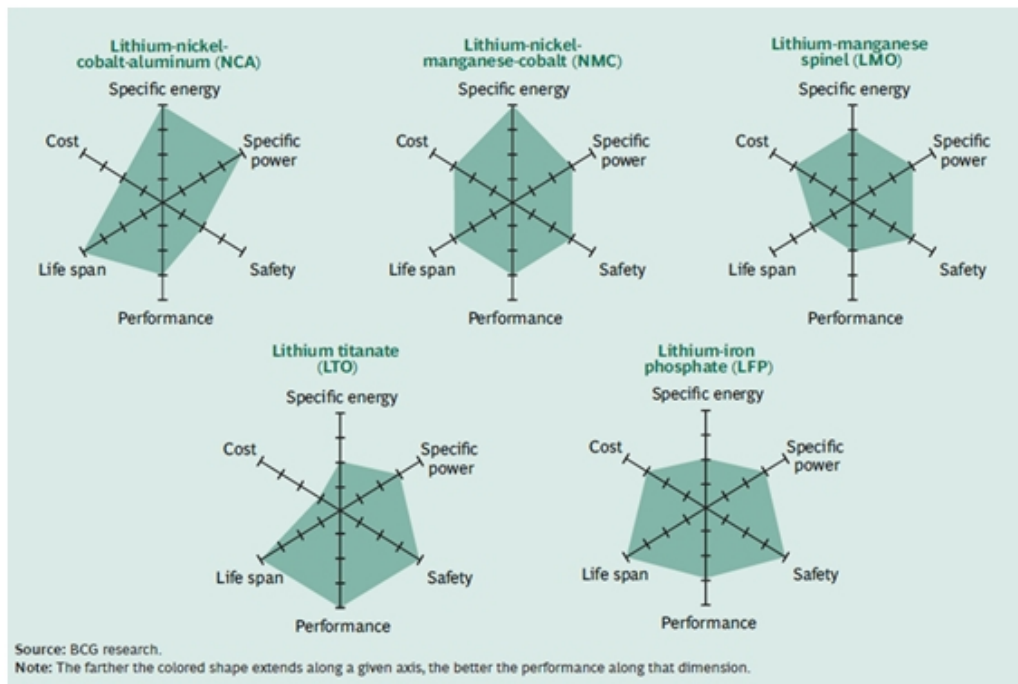


Figure 2.6: Tradeoffs among the five principal Lithium-Ion battery technologies. [BCG, 2010]

disadvantages in terms of safety, performance, cost, and other parameters.

The most prominent technologies for automotive applications are Lithium-Nickel-Cobalt-Aluminum (NCA), Lithium-Nickel-Manganese-Cobalt (NMC), Lithium-Manganese-Spinel (LMO), Lithium-Titanate (LTO), and Lithium-Iron-Phosphate (LFP). The technology that is currently most prevalent in consumer applications is Lithium-Cobalt-Oxide (LCO), which is generally considered unsuitable for automotive applications because of its inherent safety risks. All automotive battery chemistries require elaborate monitoring, balancing, and cooling systems to control the release of energy, prevent thermal runaway, and ensure a reasonably long life span for the cells. The recent explosion in innovation is driven by the need to break some fundamental compromises in battery technology. On the technical side, competing Lithium-Ion technologies can be compared along six dimensions as shown in Figure 2.6:

1. Safety;
2. Life span (both number of charge and discharge cycles and overall battery age);
3. Performance (peak power at low temperatures, SOC measurement, and thermal management);
4. Specific energy (how much energy the battery can store per kilogram of weight);
5. Specific power (how much power the battery can deliver per kilogram of weight);
6. Cost.

Currently, as shown in Figure 2.6, no single technology wins along all six dimensions. Choosing a technology that optimizes performance along one dimension inevitably means compromising on other dimensions. NCA technology, for example, is a fairly high-performance solution but presents safety challenges, whereas LFP technology is safer at the cell level but provides a

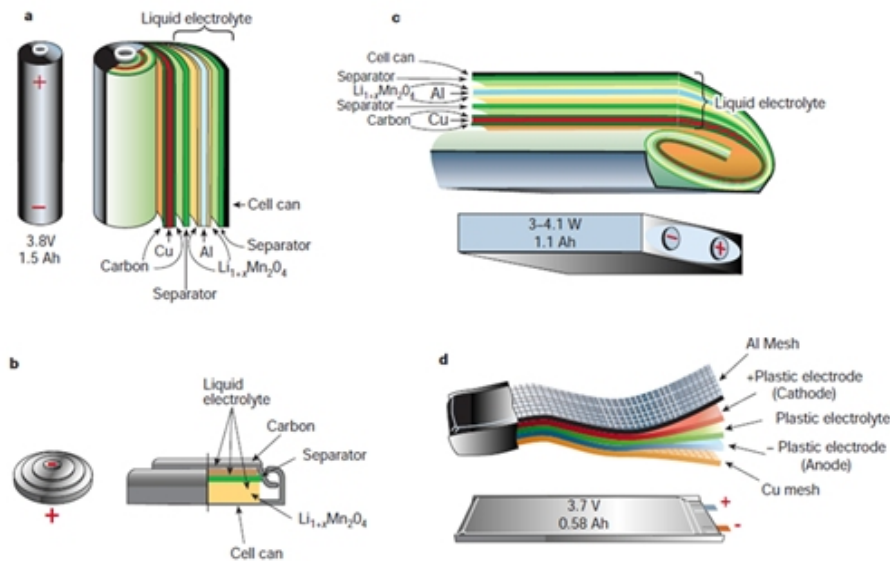


Figure 2.7: Schematic drawing of shapes and components of several Lithium-ion battery configurations: a – Cylindrical; b – Coin; c – Prismatic; d – Thin and flat. [Tarascon and Armand, 2001]

low specific energy. Other important characteristic of the Lithium-based technology is its flexibility to build batteries in several shapes and configurations, such as cylindrical, coin, prismatic and flat, as presented on Figure 2.7.

2.2.3 Battery Safety

Safety is one of the most important criterion for electric-car batteries. Even a single battery fire could turn public opinion against electric mobility and set back industry development for months or years. The main concern in this area is avoiding thermal runaway - a positive-feedback loop whereby chemical reactions triggered in the cell exacerbate heat release, potentially resulting in a fire. An overcharged battery, too-high discharge rates, or a short circuit (internal or external) can cause thermal runaway. Chemistries that are prone to thermal runaway, such as NCA, NMC, and LMO, must be used in conjunction with system-level safety measures that either contain the cells or monitor their behavior. Such measures include a robust battery box, a very efficient cooling system (to prevent the early stages of thermal runaway), and precise SOC monitoring and cell-discharge balancing. Recently, the entire fleet of Boeing Dreamliner airplanes was grounded because of a fire in a Lithium-Ion battery (Figure 2.8).

Despite the virtues of Lithium-Ion batteries, several factors have prevented a wider spread of this technology, and the most significant one is, without doubt, safety. This is mainly due to the higher energy density of those batteries, which implies more heat released in case of failure, and to the flammability of the most common organic solvents used as electrolytes. More than 2 million products containing Lithium-Ion batteries have been recalled because of battery problems since October 2006. For successfully scaling up this technology to higher



Figure 2.8: Lithium Battery from Boeing Dreamliner Airplane safety failure.

power applications like HEVs, it is imperative to reduce these concerns, i.e. to reduce the incidents and mitigate the effects of the incidents when they do occur. This is done by means of various expedients, among which a battery management system, through its thermal and charge management, plays a critical role. The dangerousness of the above-mentioned events in a particular Lithium-Ion cell highly depends on the particular chemistry of the cell. Some chemistries are more susceptible than others, and the more dangerous chemistries should be avoided for high power applications, or should be modified with appropriate additives. Each cell should be adequately insulated from the others in the battery pack, in order to avoid the danger of chain reactions causing neighboring cells to fail due to the heat exchanged between cells. It is responsibility of BMS to ensure that the cells of a battery operate within their rated specifications. This can be done, for example, through cell state monitoring, charge and discharge current limiting, cooling system management, communication between the battery system and the vehicle, and SOH estimating. In addition, avoiding high SOC levels when the temperature is high can be desirable. In fact, the higher the SOC of the cell is, the more likely the cell may fail when thermally stressed. In order to minimize the risk of safety-related failures (Figure 2.9), safeguards should be adopted redundantly and at various levels, ensuring a robust chemical and mechanical battery design, controlling the quality of the manufacturing process, and employing a satisfactory electronic supervisory system. Eventually, the development of standards to evaluate the safety performance of the resulting battery systems will prove decisive to establish Lithium-Ion batteries as safe energy storage devices, especially in the automotive field.

2.2.4 Life Span of Lithium-Ion Batteries

Life span is an important parameter of an EV battery as it impacts strongly the total cost of ownership (TCO) of the vehicle. Batteries are the heaviest component of an EV and their cost can be higher than half of the final price of acquisition. During their use, they can be subject to

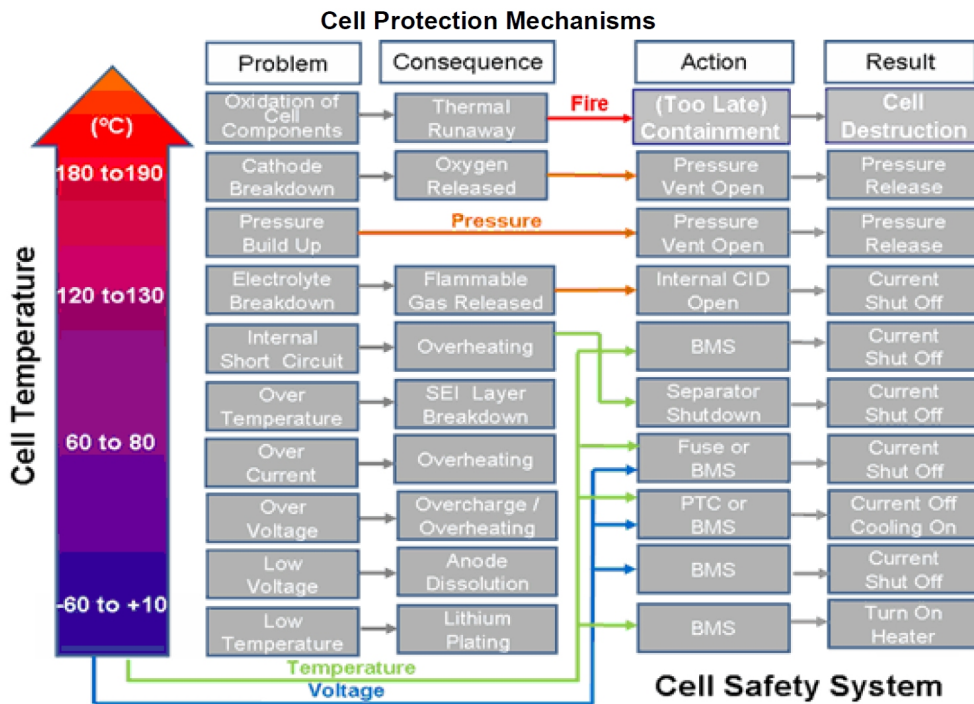


Figure 2.9: Safety failure related mechanisms on cell level. [Electropaedia, a]

different kind of stresses depending on environment conditions and driving profiles. They are especially sensitive to extreme temperature conditions or over-charge and discharge conditions. Therefore, it is important to understand the aging mechanisms of the battery in order to avoid the conditions that can speed up those effects. There are two ways of measuring battery life span: cycle stability and overall age. Cycle stability is the number of times a battery can be fully charged and discharged (80%DoD) before being degraded to 70 percent of its original capacity at full charge. Overall age is the number of years a battery can be expected to remain useful. Today’s batteries do meet the cycle stability requirements of electric cars under test conditions. Overall age, however, remains a hurdle, in part because aging accelerates under higher ambient temperatures. Yet, it is unclear how fast various kinds of batteries will age across a range of automotive-specific temperature conditions. To manage these uncertainties, OEMs are specifying batteries of sufficient size to meet electric cars energy-storage needs over the typical life of a vehicle. Most automotive manufacturers are planning for a ten-year battery life span, including expected degradation. For example, an OEM whose electric car nominally requires a 12-kilowatt-hour (kWh) battery is likely to specify a 20-kWh battery instead, so that after ten years and 40 percent performance degradation, the battery will still have sufficient energy capacity for normal operation. Of course, this approach increases the size, weight, and cost of the battery, adversely affecting the business case for EVs.

Different battery strategies can be used to preserve the battery lifetime. A conservative method could be to avoid a SOC above 80% keeping some margin for regenerative braking energy and never discharge below 80% DoD. Such a method is shown on Figure 2.10. The

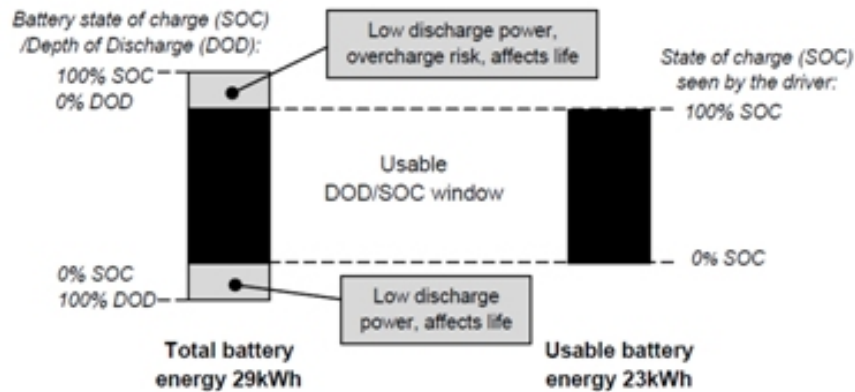


Figure 2.10: Illustration of a battery with 80% DOD/SOC window. [Energy, 2012]

drawback already mentioned is that the useful battery energy will be less than the installed battery capacity.

2.2.5 Aging Of Lithium-Ion Batteries

Unfortunately, Lithium-Ion batteries are complex systems to understand, and the processes of their aging are even more complicated. Capacity decrease and power fading do not originate from one single cause, but from a number of various processes and their interactions.

Aging in Lithium-Ion cells may mainly come from:

- Reactions of active materials with electrolyte at electrodes interfaces;
- Self-degradation of active materials structure on cycling;
- Aging of non-active components (ex: electrodes binders).

These phenomena lead to energy and/or power losses. Aging mechanisms occurring at anodes and cathodes differ significantly. The influence of the electrolyte and the aging of the electrolyte itself (and the separator as well) mainly take place at the electrodes and in interaction with them:

- On the negative electrode side, the main parameters are passivation layer stability, the layer structure/composition (effect of additives in electrolyte and formation process) and polluting agents;
- On the positive electrode side, key factors seem to be the material structure evolution and organic solvent oxidation.

These phenomena are highly dependent of voltage and temperature.

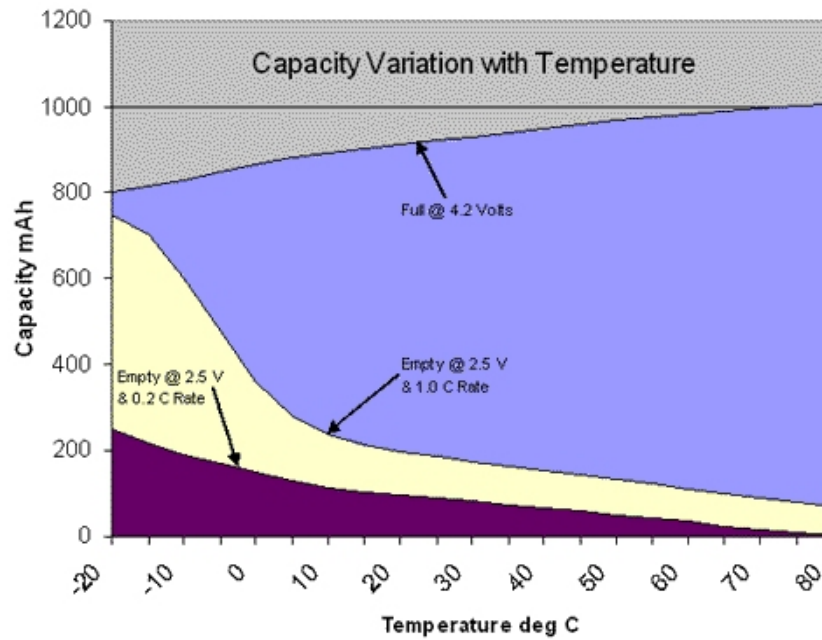


Figure 2.11: Capacity variation with temperature. [Electropaedia, b]

2.2.6 Performance of Lithium-Ion batteries

2.2.6.1 Efficiency

During the charge, some of the energy is inevitably lost in the chemical conversion process usually as heat. Similarly on the return trip, for the same reasons, some of the available charge is lost and only part of the stored charge is available for doing work. The round trip energy loss is about 3% for a Lithium-Ion battery. The efficiency is the ratio between the discharge energy and the charging energy. The battery efficiency and capacity will change depending on charging and discharging parameters. The typical charge and discharge characteristics are usually part of the battery specifications.

2.2.6.2 Capacity Change with Temperature and Discharge Rate

Figure 2.11, shows how the capacity of a Lithium-Ion cell varies with temperature and discharge rate. It shows that at normal working temperatures, the efficiency of the cell is very high, but at low temperatures, there is a major drop in efficiency particularly at high discharge rates, which can give rise to serious errors in the estimation of the SOC. This phenomenon is not peculiar to Lithium cells as other cell chemistries also demonstrate deterioration in performance at low temperatures.

The discharge rate (C or C-rate) of a Lithium-Ion cell is typically the current needed to discharge a fully charged cell in one hour. Its value, in ampere units, is calculated from the specified cell capacity in ampere-hours divided by one hour time.

The Lithium-Ion cell is working between its specified upper and lower voltage cut-off limits

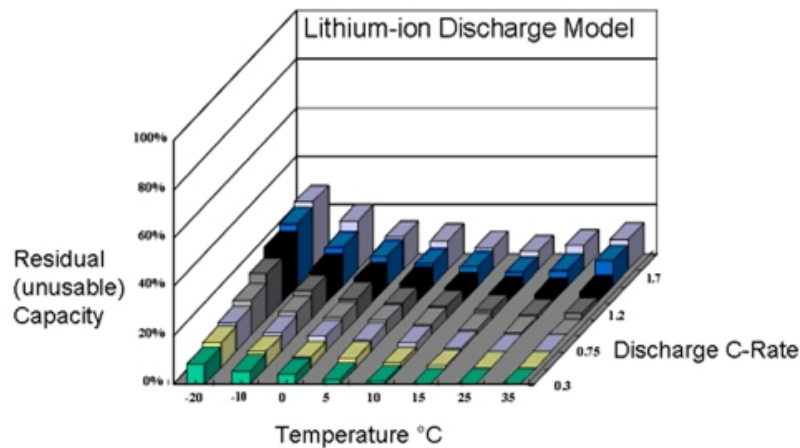


Figure 2.12: Capacity reduction at different temperatures and discharge rates. [Electropaedia, b]

of 4.2 Volts and 2.5 Volts, respectively. These are considered the fully charged and the empty conditions of the cell. The "Full" line is the point at which the cell reaches full charge using the constant current - constant voltage charging method at the corresponding temperature. Two "Empty" lines are shown corresponding to two different discharge rates 0.2C and 1.0C. The capacity of the cell at a given rate and temperature is the difference from the "Full" line and the corresponding "Empty" line. Note that the cell is very inefficient at giving up its charge at high discharge rates and low temperatures. In other words, its efficiency deteriorates dramatically at low temperatures. Note also that the cell above could be fully discharged at the high current rate yet could be further discharged at the low current rate by the number of milliamp-hours between the two "Empty" points that correspond to the present cell temperature. Typical cell specifications only give the capacity at 25°C and 0.3C rate. Figure 2.12, characterizes the performance of a Lithium-Ion cell over two of its expected operating conditions (temperature and discharge rate). The matrix of capacity values associated with all the possible current-temperature combinations is useful as a look up table used by charge estimation algorithms of a BMS.

2.3 Battery Management Systems

As EVs are evolving fast, the batteries need to improve and adapt to the stringent requirements of automotive EV. The BMS is a critical part of EVs, to guarantee that batteries operate safely and last longer. In fact, the total cost of ownership of an EV is influenced by the needed installed capacity but also by the time it remains usable. The BMS costs only a fraction of the total investment but guarantees its lifetime. The BMS architecture can be split in two fundamental parts:

- **the hardware** that acquires the state variables of the batteries: voltage, current and temperature. It should ensure the simultaneous acquisition of the measurements in order

to improve the accuracy of the estimations. It needs a high sampling rate to guarantee that the system dynamics can be monitored and it needs to accurately measure the electrical and thermal variables in order to avoid error propagation and to allow a reliable estimation of all the parameters that are not measurable directly.

- **the software** that actively monitors all the variables, manages the battery protections and alerts, manages the internal communication within the different hardware blocks, manages the communication with the peripheral systems and implements estimation or cell balancing algorithms.

There are different approaches for the hardware that can be centralized or distributed with advantages and disadvantages for each situation.

Also the modeling of the cell is an important part of the BMS. Models can be as simple or as complex as required. Since a simple voltage source and series resistor to electrochemical models that represent all the interactions on the battery molecular structures.

The experience from the author reveals that most commercial BMS available rely on the most simple estimation procedures to calculate most of the parameters. The coulomb counting technique and voltage drift offset are used on the ORION BMS [ORION, 2014]. The main disadvantage from coulomb counting method, is the fact that it needs always a known starting point because the current integration over the time will accumulate errors that can become substantial if a complete charge or discharge do not occur.

Lithium-Ion batteries are already available for many years for portable devices such as laptops and mobile phones. Also BMSs for those devices are available from different IC manufacturers and are already mature. Those ICs are not suited for EV Battery pack because they can range from tens to more than hundred cells to provide a high power system needed for traction. Those systems with high voltage and high currents impose additional communication signal isolation for devices interface, and are still under strong development by companies, car manufacturers, research institutes and universities [Xing et al., 2011].

The energy crises of the 1970s and 1980s brought a renewed interest in EVs [Wikipedia,]. They were re-introduced in the early 1990s and became mainstream in the 2000s leading to breakthroughs in battery technology. Lithium-Ion technology has been widely adopted for EV/HEV applications due to its high energy density and power density, low self-discharge and long life span [Tao et al., 2011]. It faced an enormous improvement on the last decade. Unfortunately the BMS developments could not follow those developments hindered by the following difficulties, among others [Xing et al., 2011]:

- Battery modeling;
- Battery state estimation (SOC, SOL, SOH);
- Cell balancing.

The basic functions of a generic BMS can be summarized as it follows:

- Measure the battery state parameters like, individual cell voltages, pack current and temperature;
- Trigger alarms in case of abnormal conditions or even act to disconnect the batteries in order to avoid damaging failures;
- Control charge and discharge conditions;
- Cell balancing;
- Thermal management;
- Estimation and communication of important battery parameters like SOC, SOH, SOL.

Not all those functions are available on current commercialized BMSs. Also those functions are not standard. Table 2.1 compares some popular marketed products.

Table 2.1: Comparative analysis of commercially available BMS ICs.

Manufacturer/Part Number	Maxim/MAX14921 [Maxim, 2014]	TI / BQ76PL536 [BQ76PL536,]	AMS/AS8506 [AS8506,]
Description	3-16 cell analog front end scalable to any number of cells	3-6 cell analog front end plus fault detector scalable to 192 cells	7-cell analog front end scalable to any number of cells
Measured Cell Parameters	voltage, current	voltage, current	voltage, current
Measured Pack Parameters	temperature, pack voltage	temperature	temperature
Safety Protection	open-wire detection undervoltage/overvoltage alarms	over and undervoltage protection, overtemperature protection	cell voltage diagnosis
Communication	SPI	SPI	SPI
Passive cell balancing	integrated cell-balancing FET drivers - Simultaneous	control outputs with balance current set by external components	internal FET- Sequential balancing, 50mA max.
Active cell balancing	N/A	N/A	option for active charge balancing with external components - DC-DC Flyback
Internal ADC	No	Yes. 14 bits SAR	Yes. 12 bits SAR

Those products have the following limitations:

- No self data logging capabilities. This is an important feature for storing the driving patterns in order to build up and update the SOC model;
- Lack of State Of Health (SOH) and State Of Life (SOL) estimations. This is useful to characterize the performance of the battery and schedule the battery replacement or repair;
- No interchangeability among current BMSs as they all have different pin-outs, different cell balancing schemes, different communication channels between BMS ICs and between BMS IC and host controller.

2.3.1 Battery Modeling

There are nowadays several types of battery models ranging from simple electrical equivalent circuits (EEC) to complex electrochemical models that try to model the molecular reactions inside the cell. Both have advantages and limitations as shown on Table 2.2.

Table 2.2: Advantages and limitations of existing Lithium-Ion modeling methods. [Antaloae et al., 2012]

Modeling Method	Accuracy	Setup simplicity	Run-time performance	Type of method
Coulomb counting	★★	★★★★★	★★★★★	offline
Direct voltage measurement	★	★★★★★	★★★★★	offline
Impedance measurement	★★★	★★	★★★★	offline
Electrode electrochemistry	★★★★	★	★	offline
Equivalent electrical circuit (EEC)	★★	★★★★	★★★★	offline
Adaptive methods (KF,EKF,ANN,FL)	★★★★★	★★	★	online

They can be categorized in two main classes:

- offline methods - derive the model parameters from analysis of available datasets. Most of the times this data is measured in laboratory under controlled conditions. This data should reflect the real application and environment conditions so it usually lead to extensive testing. Since it is virtually impossible test all the real conditions, approximations need to be done.
- online methods - use an adaptive approach to update the model parameters as the battery is being used. Those methods lead to improved accuracy in detriment of increased complexity and reduced run-time performance.

All those methods are extensively mentioned in the literature.

The coulomb counting [Ng et al., 2009] [Piller et al., 2001], direct cell voltage measurement [Coleman et al., 2007], impedance measurement [Huet, 1998], electrode electrochemistry [Bergveld, 2001] and equivalent electrical circuit [Schweighofer et al., 2003] [Chen and Rinc, 2006] [Antaloae et al., 2012] [Huria et al., 2010] are examples of offline methods. The Kalman Filter, Extended Kalman Filter [Plett, 2004], Artificial Neural Network [Parthiban et al., 2007] and Fuzzy Logic [Salkind et al., 1999] are examples of online adaptive methods.

2.3.2 Cell Balancing

Cell balancing is an important part of any Battery Management System. There are not two cells exactly the same. Even cells manufactured under the same conditions and coming from the same batch can have minor changes due to their electrochemical nature. Typical battery packs for EVs can have more than one hundred cells. Depending on how those long strings are mounted, some cells can have slightly different temperature conditions during operation. Also in stationary mode those differences can exist due to environmental conditions. The self-discharge rate of Lithium-Ion cells is very dependent on temperature. So the differences among cells tend to increase with normal cycling and aging, leading to an unbalance on the SOC of the cells.

Since the cells are in series, they share the same current. This means that the cell with higher SOC will reach its maximum terminal voltage before the others can reach full charge. On the other way, the cell with lowest SOC will reach its minimum voltage on discharge before the other ones can deliver its full capacity. Continuing with the charge or discharge in those conditions will lead to overcharge of the cell with highest SOC or over-discharge of the cell with lowest SOC. In this way the useful capacity will be lower than the rated capacity.

Then, in order to establish safe operation, maximize battery life and optimize its useful capacity, proper individual cell balancing should be achieved [Kuhn et al., 2005].

The balancing topologies can be categorized as passive and active balancing. The passive balancing methods act removing the excess charge from the most charged cell(s) through a passive resistor element, until the charge matches those with lowest charge in the pack. The resistor element will be either in fixed mode or switched. The active cell balancing methods remove charge from the most charged cell(s) and deliver it to lowest charged cell(s). Different topologies are used according to the active element used for storing the energy such as capacitor and/or inductive component as well as controlling switches or converters. The different solutions vary in complexity, efficiency and response time. An overview of the different configurations available on the literature [Daowd et al., 2011] can be found in Figure 2.13.

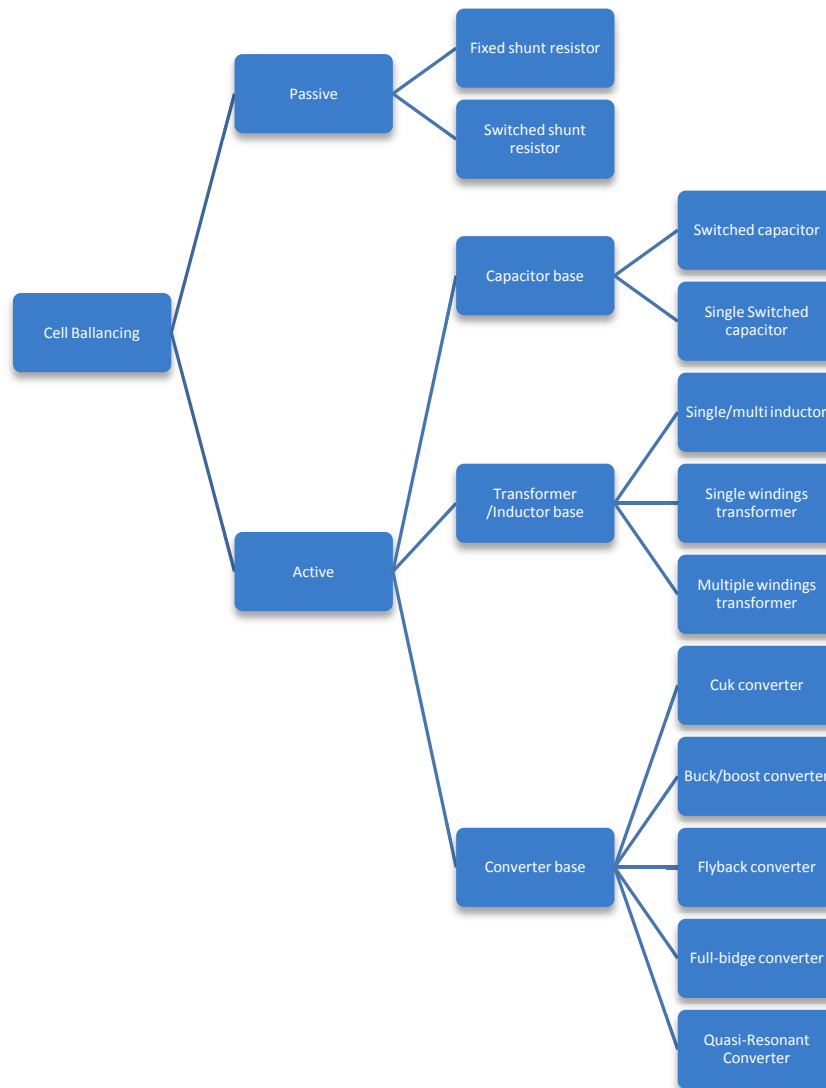


Figure 2.13: Cell balancing topologies.

A comprehensive revision on cell balancing is provided by [Cao et al., 2008] and is summarized by [Rahimi-eichi, 2013] on Table 2.3.

Table 2.3: Comparison of different cell balancing methods. [Rahimi-eichi, 2013]

BALANCING TECHNIQUE	BALANCING TECHNIQUE	PROS	CONS
Passive	Cell-to-heat (one bleeding resistor and switch per cell)	Very simple	0% efficiency
		Very cheap	Slow (limited by the maximum allowable dissipated power on board)
Active	Module-to-cell (charge transfer from a battery module to a single cell by means of a galvanic isolated dc/dc converter)	Relatively simple	Switch network
		Good efficiency	High isolation voltage of the dc/dc
		Fast	
Active	Cell-to-cell		
	Cell-to-cell distributed (charge transfer from adjacent cells)	Moderate efficiency	Bulky
	Cell-to-cell shared (charge transfer from cell A to tank, then from tank to cell B)	Moderately fast	Complex control
		High efficiency	Switch network
		Fast	
Active	Cell/module bypass (a cell/module disconnection from the current path)	High balancing efficiency	High current switches
		Very fast and flexible	Complex to implement Decrease battery efficiency during operation

Chapter 3

ISR-Battery Management System

In this chapter, the architecture of the ISR-BMS is presented and the choices undertaken are fundamented. The whole design process and key features are presented along the developed hardware and software.

3.1 Preliminary Work

An example of the EVs used on this project is shown in Figure 3.1. Those are derived from a Yamaha electric AGV that was re-instrumented at ISR-UC. [Silva et al., 2012]



Figure 3.1: ISR-UC Electric Vehicle

The original platforms were equipped with Lead Acid batteries that reached the end of life. At the beginning of this work the following equipment was available to be installed on the first re-instrumented platform:

1. Lithium-Ion battery pack acquired to the company Autosil S.A., shown in Figure 3.2.



Figure 3.2: Lithium-Ion battery pack acquired to the company Autosil S.A. (72V, 3kWh, 24 modules in series with 4 parallel cells each - 4P24S).

2. A commercial BMS from ORION manufacturer with CAN interface, shown in Figure 3.3.

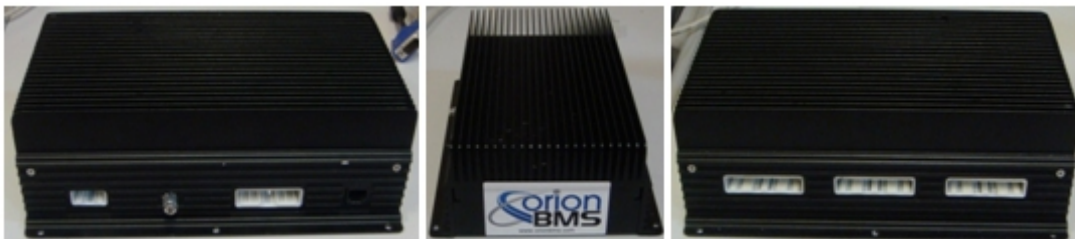


Figure 3.3: ORION BMS.

3. A 1.5kW Battery charger from TC Charger, shown in Figure 3.4.



Figure 3.4: TC Charger.

The first task in this work was to integrate the ORION BMS with the Autosil battery pack and the TC Charger. This involved all the wiring and the parametrization of the BMS to the used cells and charger.

After integration, the system was extensively tested in the lab to check among other parameters the battery capacity, the BMS indications, the charge and the cell balancing. To discharge the cells a bank of resistors with configurable resistance was used as shown in Figure 3.5.



Figure 3.5: Battery test setup.

After the first two preconditioning charge/discharge cycles, was concluded that the battery pack was completely unbalanced. At discharge, 2 cell groups (11 and 18) were reaching the cut-off voltage (2.8V) much faster than the average, limiting the useful capacity of the battery on discharge. This can be seen on the discharge log shown in Figure 3.6.

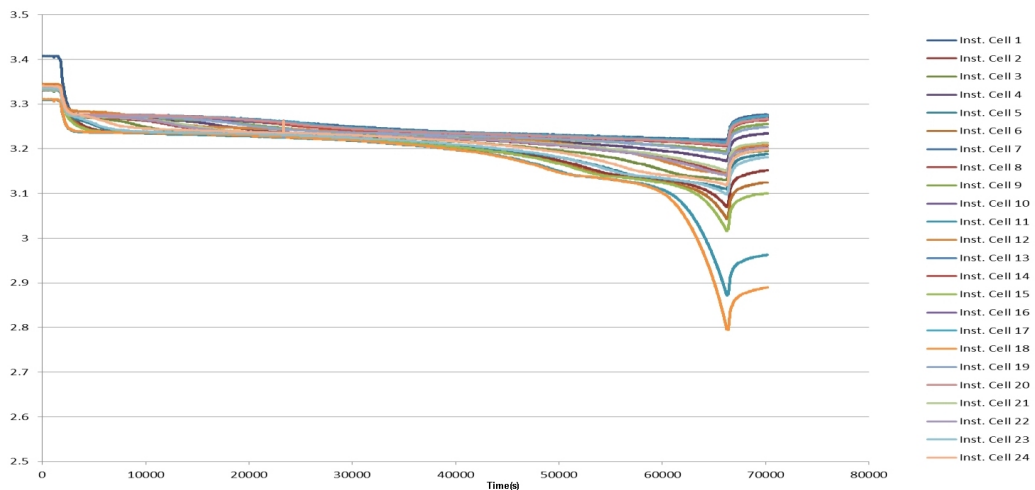


Figure 3.6: Discharge logging of Autosil battery pack constant current discharge (15A).

The same behavior could be seen during the charge, where cell 1 clearly was reaching the maximum charge voltage (3.65V) before all the others.

Due to this unbalance on the cells SOC, only 2/3 of the total battery pack capacity (40Ah) could be effectively used. The ORION balancing feature was used for one full day without visible results because the maximum balancing current is only 200mA. This current is enough for regular balancing but not suitable for highly initial unbalance.

The solution was to completely charge every cell individually with a CC/CV profile. To accomplish this, the battery pack was unmounted to access the battery terminals and power supplies were attached sequentially to every cell controlling the charge at 2A till maximum charge voltage could be reached (CC) and waiting the required time to the charge current fall below 100mA (CV).

This procedure, besides being time consuming, was also risky since all the setup was manipulated with live voltages accessible, where the smallest unintentional mistake could give rise to a short-circuit of the pack cells (partial or total) originating currents of several hundred Amperes and high probability of material and personal injury.

3.1.1 Energy Storage System selection for the new developed platform

The EV was equipped with 6 Lead Acid batteries of 12V (72V-78V) with a capacity of 60Ah that became end of life and needed to be replaced.

The choice for a Lithium-Ion chemistry was taken based on their advantages comparatively to lead acid batteries, such as high-power density, high energy density, high efficiency, no memory effect and low self discharge.

Within the lithium chemistry, the choice was based on safety, form factor, easiness of installation, suitability for the power train requirements, cost and availability.

Since the battery pack and BMS needed to be assembled in house, single cells with higher capacity were preferred in comparison with multiple parallel cells to reach the same capacity. Also the prismatic shape could fit better on the compartment reserved for the battery. This translates in less terminals (connection bars), less screws, so less probability of bad connections or high-impedance paths within the battery pack.

The final choice was also influenced by the availability at ISR of 12 cells of LiFeYPO₄ from Winston manufacturer, with a capacity of 90Ah and a nominal voltage of 3.2V. The cell datasheet can be found on Appendix D. Those cells were used in a previous project and were in good condition. Since the same model could be bought in Europe with fast delivery, this cell model was chosen to power the new platform. The remaining 12 cell units needed to reach the required power train voltage (24 cells in series) plus 4 units to be used as auxiliary battery for the instrumentation were acquired. The Battery pack prior to the BMS installation as well as the instrumentation battery can be seen in Figure 3.7.

The effect of mixing brand new cells with already used cells represents an additional challenge to the developed BMS. In fact this represents a real situation where one cell can become

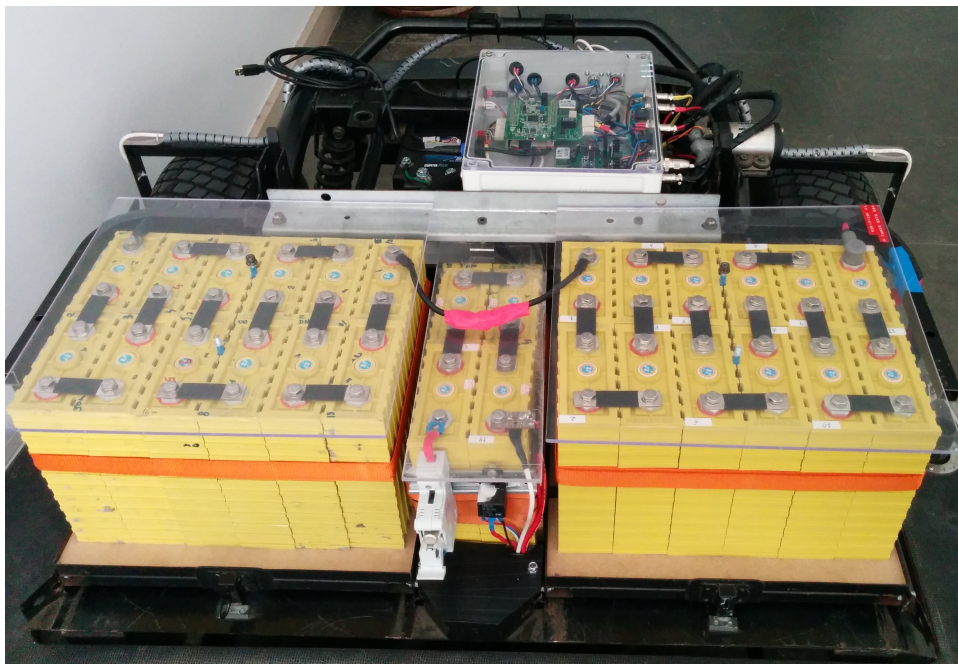


Figure 3.7: Energy Storage System of the newly developed platform

damaged and needs to be replaced, while the remaining cells are still in a good condition.

3.2 BMS requirements

Due to the limitations found on commercial available BMSs it was decided to develop a new BMS module from the scratch using available blocks from main IC manufacturers and add the required “intelligence” and flexibility to test different charge, discharge, cell ballancing and parameter estimation algorithms.

The preliminary requirements were then defined and include:

- Interface USB;
- Graphical User Interface (GUI) for parametrization and monitoring;
- Data logging;
- Programmable CAN Interface (J1939);
- Galvanic Isolation from Power battery;
- Passive cell balancing with proprietary algorithm;
- High sampling rate;
- Voltage measurement accuracy: 1-2mV;
- Current measurement accuracy: 300mA;
- Very low consumption;
- Thermal management.

The main architecture was then outlined as shown in Figure 3.8.

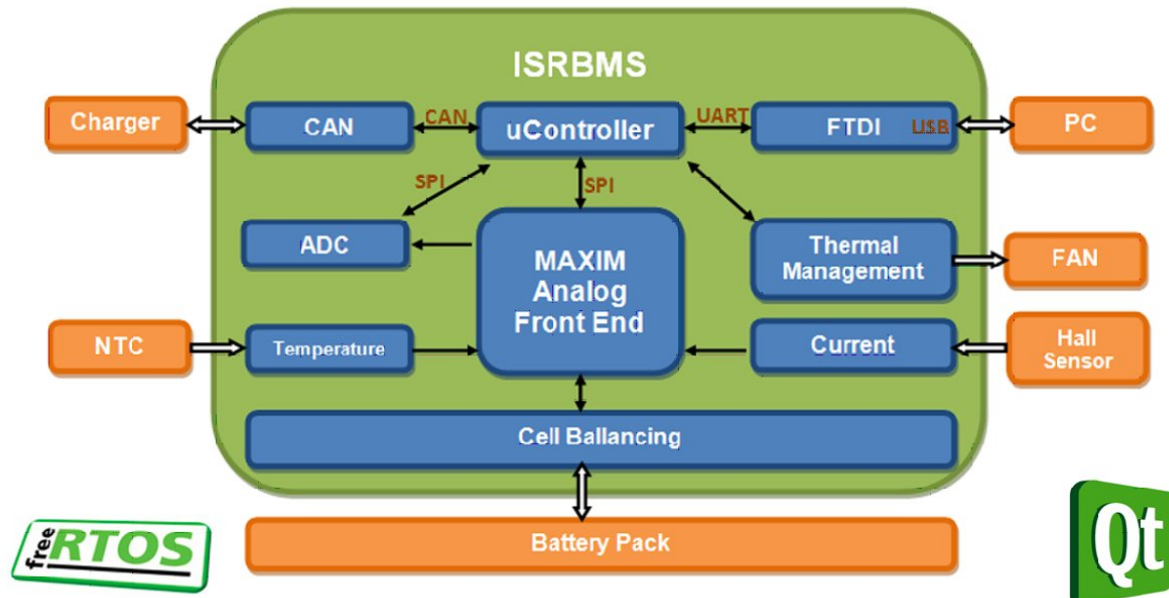


Figure 3.8: ISR-BMS Architecture

3.3 ISR-BMS Development

The complete development can be divided in three main components:

1. The Hardware - includes the PCB, components, enclosure, cables.
2. The Firmware - includes the embedded programming for the microcontroller to perform and acquire all the measurements and manage the communication with the PC (USB) or the charger (CAN). To manage the complexity and optimize the task scheduling, a real time operating system was used (freeRTOS). The program was developed using the C language and a C18 compiler.
3. The GUI - for easy and intuitive parametrization of the BMS a PC GUI was developed. This software was built in QT, a cross-platform application framework for developing graphical applications, using C++. It features real-time data acquisition and plotting.

The ISR-BMS is often referred simply as BMS during this section to avoid the prefix repetition.

3.3.1 Hardware

The hardware development workflow is represented in Figure 3.9. The main hardware blocks of the BMS are explained in detail on the following subsections.

A complete Schematic diagram can be found in Appendix A.

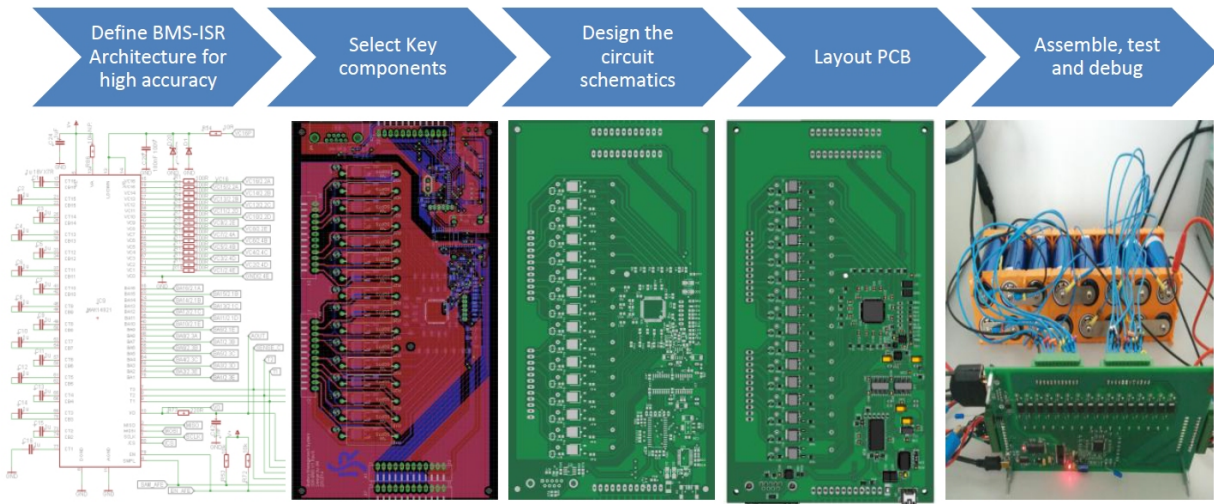


Figure 3.9: Hardware development workflow.

3.3.1.1 The MAX14921 Analog Front End(AFE) Integrated Circuit

The ISR-BMS is built around an high accuracy 16-cell Analog Front End (AFE) IC, the MAX14921 [Maxim, 2014] from MAXIM INTEGRATED. This IC is able to sample all the cell voltages simultaneously and provides level shifting for battery packs up to 16 cells / 65V(max). All cell voltages are level shifted to ground reference with unity gain simplifying external ADC data conversion. The device includes a low-noise, low-offset amplifier that buffers differential voltages up to +5V, allowing monitoring of all common Lithium-Ion cell technologies. The resulting cell voltage error is $\pm 0.5\text{mV}$, what makes it ideal to monitor cell chemistries with very flat discharge curves, such as Lithium Iron Phosphate (LiFePO₄). A comparative analysis of cell voltages of different chemistries can be seen in Figure 3.10.

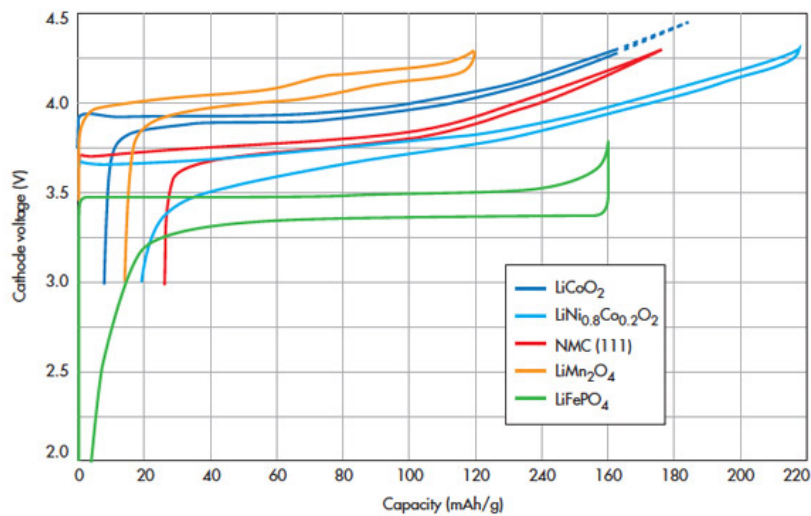


Figure 3.10: Battery voltages with different cathode chemistries. [Electronicdesign, 2012]

The MAX14921 key features can be summarized as follows:

- High accuracy
 - $\pm 0.5\text{mV}$ (max) Cell Voltage;
 - Simultaneous Cell Voltage Sampling;
 - Self-Calibration.

- Integrated Diagnostics
 - Open Wire and Short Fault Detection;
 - Undervoltage/Overvoltage Warning;
 - Thermal Shutdown.

- High Flexibility
 - SPI Interface;
 - Up to 16 Cell per IC;
 - +6V Minimum (3 Cells) Operation;
 - +0.5V to 4.5V Cell Voltage Range;
 - Integrated Cell-Balancing FET Drivers.

- Low Power
 - $1\mu\text{A}$ Shutdown mode;
 - $1\mu\text{A}$ / $10\mu\text{A}$ Cell Current Draw.

In applications requiring more than 16 cells, multiple BMS modules can be stacked. Each model can monitor any number of cells between 3 and 16 Cells. The stacked models can communicate through SPI. To translate the inter-pack communication signals between different common-mode pack voltages, digital isolators are required.

The performance of the system in which the MAX14921 is used depends highly on the components that support and surround it [Georges, 2014].

The developed architecture requires high accuracy and resolution to accurately measure very flat discharge voltage curve characteristics like is the case of Lithium Iron Phosphate cells.

Table 3.1 [Georges, 2014] shows a cost/performance comparison based on different possible architectures using the MAX14921 AFE.

The chosen topology (accuracy optimized) is represented in Figure 3.11.

Table 3.1: Cost/performance comparison of possible alternative BMS architectures.

Architecture	Relative Cost	Three-Sigma Error	Six-Sigma Error	Circuit Topology
Accuracy-Optimized	High	1.087mV	1.714mV	External ADC(16 bit), external compensated voltage reference
Accuracy-Optimized, Cost-Reduced	Medium-High	5.014mV	7.305mV	External ADC(16 bit) with internal voltage reference
Cost-Optimized, Accuracy-Enhanced	Medium-Low	17.632mV	31.154mV	Microcontroller with integrated ADC(12 bit) and external voltage reference
Cost-Optimized	Low	161.849mV	251.307mV	Microcontroller with integrated ADC(12 bit) and reference derived from a voltage divider

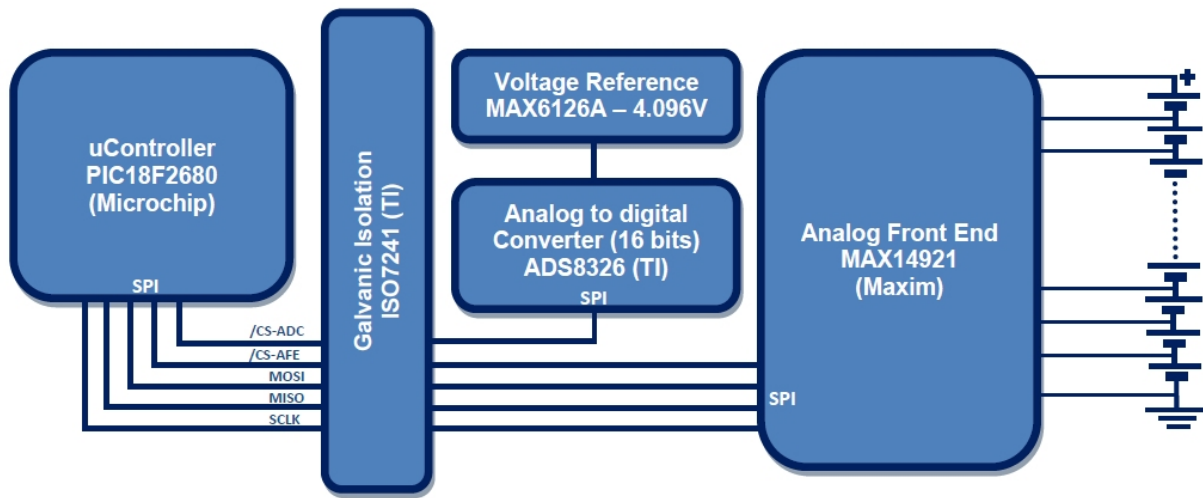


Figure 3.11: ISR-BMS Architecture.

The key components can be identified on the circuit board developed, shown on Figure 3.12.

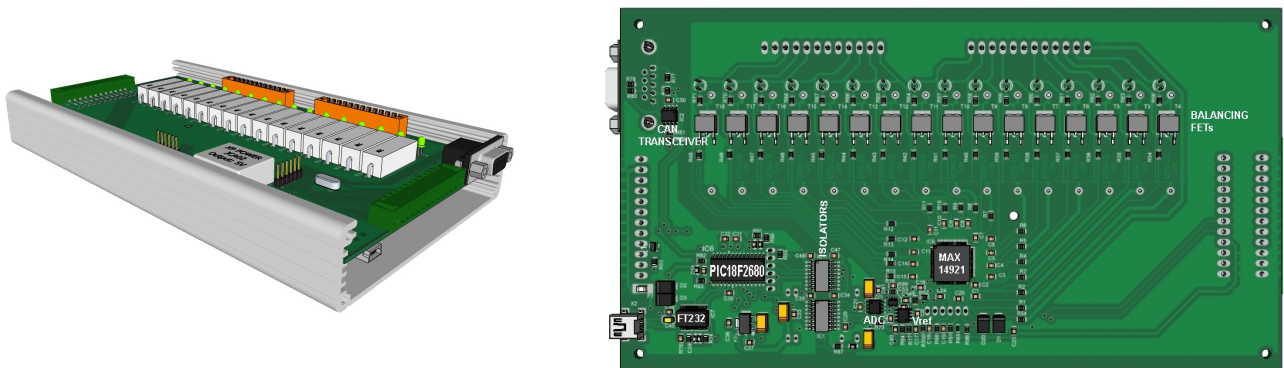


Figure 3.12: Circuit Board bottom side derived from Eagle Layout Software.

The MAX14921 integrates gate drivers to interface external mosfets enabling passive cell balancing. Each cell mosfet enables balancing through a current shunt resistor. The balancing current was set to about 200mA for a balancing voltage of 3.5V.



Figure 3.13: HTFS200 - Hall-effect current sensor from LEM manufacturer.

3.3.1.2 BMS Microcontroller

The microcontroller was chosen based on its available peripherals (SPI, UART, CAN), simple 8-bit architecture, low power consumption and available program and data memory (including its non volatile EEPROM).

The selected IC is a PIC18F2680 from Microchip Technology Inc. This is an enhanced flash microcontrollers with ECAN™ Technology, 10-Bit A/D and nanoWatt Technology.

3.3.1.3 Current Sensor

Current measurements must be carried out with high accuracy as they represent the primary input for most SOC estimation algorithms.

The battery pack installed on the EV is able to supply a nominal current of 270A (3C). The traction motor on the platform is a 3.5kW DC Motor with separated excitation. In road tests, peak powers of 11kW were observed. Considering an average voltage of 3.2V per cell (76.8V for complete pack) this gives a peak current of 143A. This can change based on the battery pack SOC.

To accommodate some margin also for the foreseen power train evolution from the current DC motor to a permanent magnet DC motor with higher power, the current sensor rate was set to 300A.

The selected sensor is a LEM HTFS200 based on the hall-effect measuring principle.(Figure 3.13)

A typical accuracy target for current measurements ranges between 0.5 and 1%. For this application with a current range of 150A this translates to an accuracy of 0,75 to 1.5A. Since the average battery current consumption for this vehicle is about 30A this would lead to unacceptable errors and therefore the current measurement setup targets an accuracy of 300mA over the whole range taking in account the linearity error, voltage offset error and temperature coefficient errors from the sensor datasheet.

To accomplish this accuracy an initial current calibration procedure is run every time the BMS is started that eliminates any voltage offset from sensor.

3.3.1.4 Temperature Sensor

The thermal management is an essential part of every BMS as temperature heavily affects the performances of the battery. Parameters like internal resistance and capacity are temperature dependent.

For temperature measurements the chosen sensor was the 10kOhm NTC model ERTJ1VG103FA from Panasonic with 1% tolerance and a measurement range of -40°C to 125°C. This resistor varies non-linearly with temperature and this correlation is usually stored in the program memory or other kind of non-volatile memory of the microcontroller. Another approach is to linearize the curve for smaller temperature ranges where the error can be acceptable and use a linear equation to let the microcontroller calculate the temperature based on the measured voltage across the NTC as part of a voltage divider. Was followed the latest approach. And accurately approximated the characteristic NTC curve for the temperature range of 0 to 40°C.

3.3.1.5 Communication Interface Hardware - USB

The BMS can communicate via USB, using a standard mini-USB connector.

An FT232RL IC from FTDI is used to convert USB protocol to serial UART. The communication protocol is presented on the software section.

The serial COM port should be configured for 31250kbps, 8 bits, no parity and 1 stop bit.

3.3.1.6 Communication Interface Hardware - CAN bus

In order to ensure that a BMS can take the maximum benefits from a battery charger, a digital interface for setting instantaneous voltage and current is required. Most common available EV battery chargers (e.g. TC charger) feature a CAN bus interface for that purpose due to its robust characteristics.

The developed BMS also supports CAN bus interface for charging and balancing purposes. It features a full CAN system, implementing the CAN 2.0A or B protocol as defined in the BOSH specification.

For successful communication with the BMS the CAN bus must be configured with a bit rate of 250kbps.

3.3.2 Firmware

3.3.2.1 Real Time Operating System - FreeRTOS

The BMS firmware is programmed with C language, using the MPLAB(v8.90) Integrated Development Environment (IDE) and the C18 compiler from Microchip. For programming and debug the Pickit3 development tool from the same manufacturer was used.

The BMS needs to manage multiple simultaneous processes like communication with CAN, the serial communication via USB or the communication between the microcontroller and the AFE and ADC via SPI.

To manage this complexity and the task scheduling the FreeRTOS^{TM1} was used.

This kernel was chosen based on the following advantages:

- Is free for use, even in commercial applications;
- Provides one solution for different architectures and development tools;
- Has a minimal ROM, RAM and processing overhead;
- Is very scalable, simple and relatively easy to use.

This system allows for multi-thread operation. In FreeRTOS each thread of execution is called a ‘task’. Multi-tasking requires all tasks get scheduled to run on CPU according to some pre-determined scheme.

Tasks are implemented as C functions. The only thing special about them is their prototype, which must return void and take a void pointer parameter.

Each task is a small program in its own right. It has an entry point, will normally run forever within an infinite loop, and will not exit.

The complete list of created tasks with a brief description is presented below:

1. vComRxTask - Serial communication management task.
2. vCellsReadTask - Cell parameters reading and validation task.
3. vCANRxTask - CAN bus communication management task.
4. vCANSendInfoToChargerTask - Charger management task.
5. vComserialHeartbeatTask - Heartbeat implementation task.

3.3.2.2 Cells Voltage Measurement Procedure

As the code is quite extensive, accounting for more than 5000 lines, the implementation details are not going to be presented for all the tasks. As an example, in Figure 3.14 the cell voltages measurement procedure flowchart using the MAX14921 is presented.

The procedure implements the scheduling required for reliable and accurate operation of the AFE IC according to the manufacturer datasheet [Maxim, 2014] information. The relevant timing diagram is reproduced in Figure 3.15 for easy understanding.

An illustration of the file structure with a brief description for each file, outputted from Doxygen documentation generator tool, can be found at Appendix B.

¹FreeRTOSTM is a real time operating system developed by Real Time Engineers Ltd.

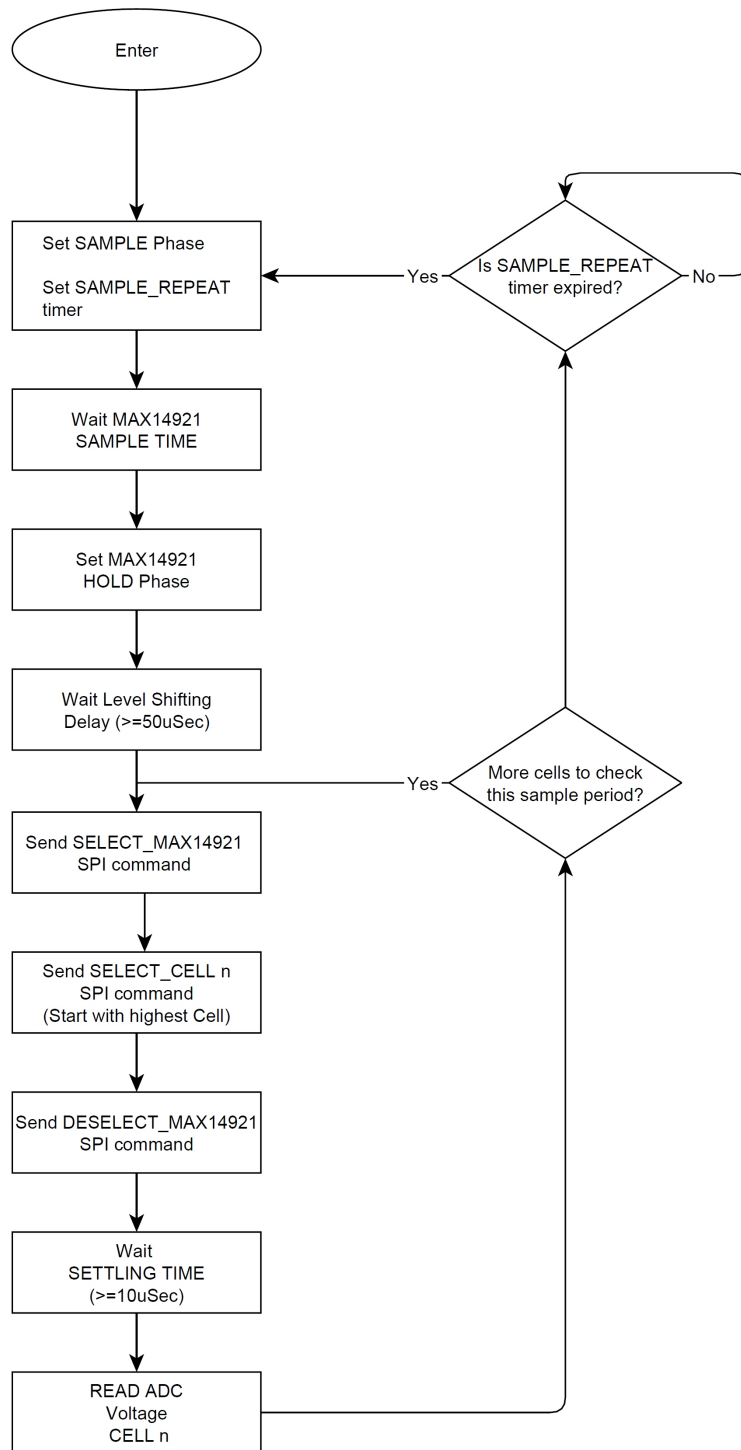


Figure 3.14: MAX14921 cell voltages measurement procedure flowchart.

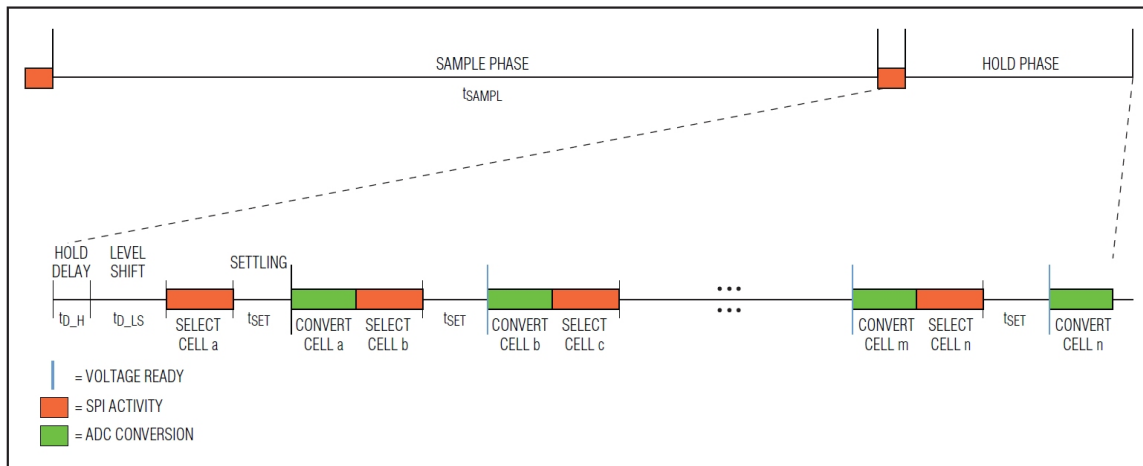


Figure 3.15: MAX14921 SPI Control of cells voltage readout.

3.3.2.3 Cell Balancing

The flowchart of the cell balancing procedure implemented in the ISR-BMS Firmware is shown on Figure 3.16.

3.3.2.4 Communication Protocol for BMS Parametrization and Data Logging

To allow the exchange of information between the PC and the BMS via serial interface, a communication protocol was developed and implemented. This protocol was designed to be flexible and easily scalable.

With the exception of the HEARTBEAT command, the communication is always started by the PC. All the commands and data exchanged are encapsulated between a START character (@) and an END character (e). The syntax of the different commands is described on Table 3.2.

The ISR-BMS features also support to OBDII via CAN bus. In this way all the relevant information from the BMS can be displayed on a tablet or smartphone with appropriated compatible software.

An example of the codes implemented and the structure of the CAN messages are shown on Table 3.3.

A screenshot of Torque software for Android implementing the readings of 7 cells plus the temperatures on the cells and on the ISR-BMS is shown in Figure 3.17. To use this feature an OBDII to bluetooth adapter based on ELM27 IC was used.

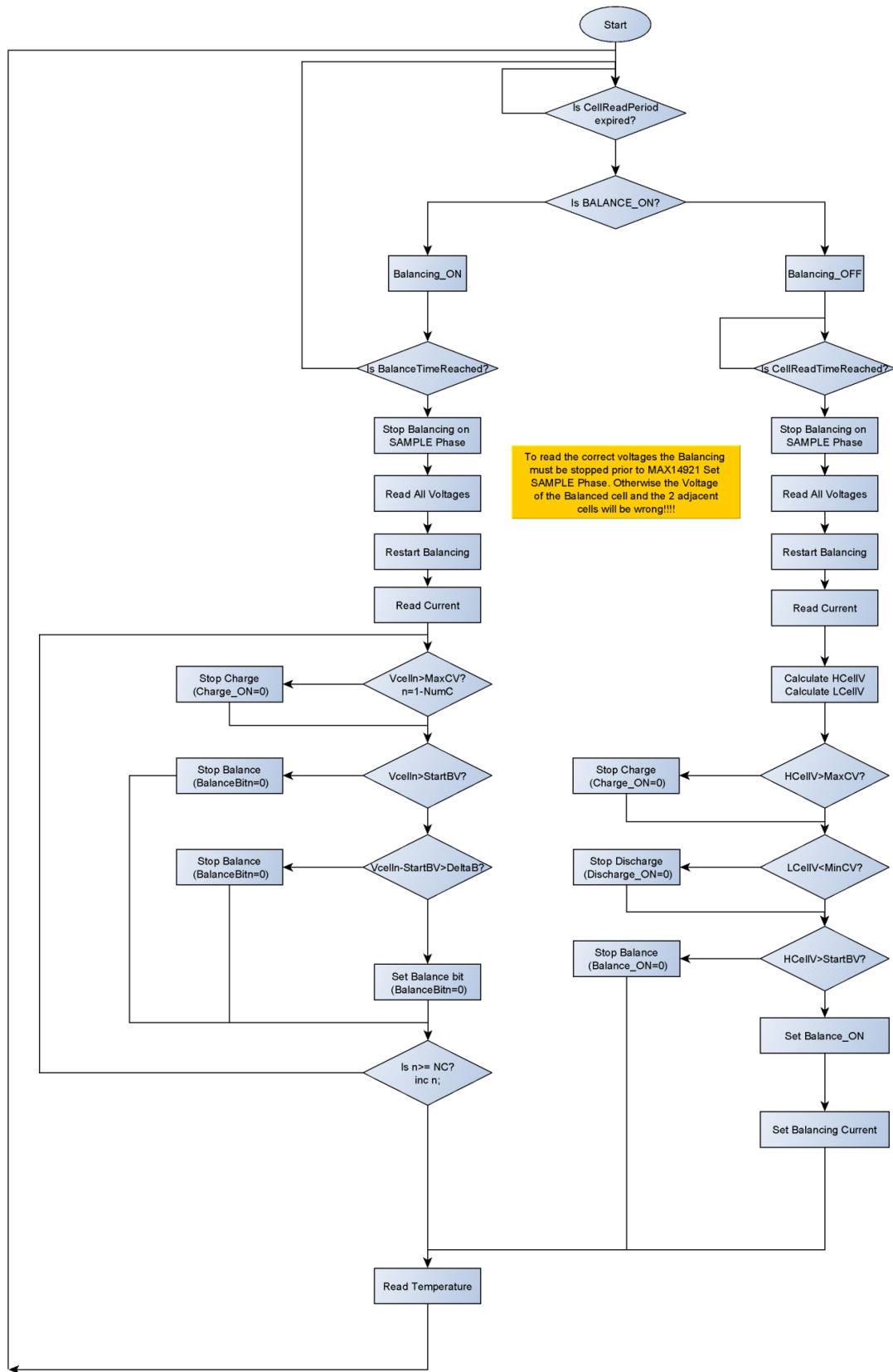


Figure 3.16: Balancing flowchart.

Table 3.2: ISR-BMS Communication Protocol

Command description	Command syntax PC (PC->BMS)	Command syntax BMS (BMS->PC)	Argument Units	Start Char	@
ASK_CELL_VOLTAGE_0	@'02'0e	@'02'1,'ARG'e	mV	Delimiter Char	,
ASK_CELL_VOLTAGE_1	@'03'0e	@'03'1,'ARG'e	mV	End Char	e
ASK_CELL_VOLTAGE_2	@'04'0e	@'04'1,'ARG'e	mV	Aux char1	'
ASK_CELL_VOLTAGE_3	@'05'0e	@'05'1,'ARG'e	mV	Aux char2	'
ASK_CELL_VOLTAGE_4	@'06'0e	@'06'1,'ARG'e	mV	Byte/Char	X
ASK_CELL_VOLTAGE_5	@'07'0e	@'07'1,'ARG'e	mV		
ASK_CELL_VOLTAGE_6	@'08'0e	@'08'1,'ARG'e	mV		
ASK_CELL_VOLTAGE_7	@'09'0e	@'09'1,'ARG'e	mV	ARG(x) with 0<x<10 stand for n comma separated Arguments	
ASK_CELL_VOLTAGE_8	@'10'0e	@'10'1,'ARG'e	mV		
ASK_CELL_VOLTAGE_9	@'11'0e	@'11'1,'ARG'e	mV		
ASK_CELL_VOLTAGE_10	@'12'0e	@'12'1,'ARG'e	mV		
ASK_CELL_VOLTAGE_11	@'13'0e	@'13'1,'ARG'e	mV	n.a - not applicable	
ASK_CELL_VOLTAGE_12	@'14'0e	@'14'1,'ARG'e	mV		
ASK_CELL_VOLTAGE_13	@'15'0e	@'15'1,'ARG'e	mV	Arguments are sent as ASCII characters	
ASK_CELL_VOLTAGE_14	@'16'0e	@'16'1,'ARG'e	mV		
ASK_CELL_VOLTAGE_15	@'17'0e	@'17'1,'ARG'e	mV		
ASK_CELL_VOLTAGE_16	@'18'0e	@'18'1,'ARG'e	mV		
ASK_TEMPERATURE_1	@'19'0e	@'19'1,'ARG'e	°C x 10		
ASK_TEMPERATURE_2	@'20'0e	@'20'1,'ARG'e	°C x 10		
ASK_TEMPERATURE_3	@'21'0e	@'21'1,'ARG'e	°C x 10		
SET_CELL_BALANCING	@'22'1,<XXXX>e	@'22'0e	n.a.		
ASK_SERIAL_NUMBER	@'24'0e	@'24'1,'ARG'e	n.a.		
SET_HEARTBEAT	n.a.	@'25'0e	n.a.		
ASK_CELLS_0_TO_7	@'26'0e	@'26'8,'ARGs(8)'e	mV		
ASK_CELLS_8_TO_15	@'27'0e	@'27'8,'ARGs(8)'e	mV		
ASK_CELLS_16_TO_23	@'28'0e	@'28'8,'ARGs(8)'e	mV		
ASK_CELLS_24_TO_31	@'29'0e	@'29'8,'ARGs(8)'e	mV		
ASK_MAX_VOLTAGE	@'30'0e	@'30'1,'ARG'e	mV		
ASK_MIN_VOLTAGE	@'31'0e	@'31'1,'ARG'e	mV		
ASK_CURRENT	@'36'0e	@'36'1,'ARG'e	mA		
ASK_PACK_VOLTAGE	@'38'0e	@'38'1,'ARG'e	mV		
ASK_INPUTS	@'39'0e	@'39'1,'ARG'e	n.a.		
ASK_TC_CHARGER_VOLTAGE	@'40'0e	@'40'1,'ARG'e	mV		
ASK_TC_CHARGER_CURRENT	@'41'0e	@'41'1,'ARG'e	mA		
ASK_TC_CHARGER_STATUS_FLAGS	@'42'0e	@'42'1,'ARG'e	n.a.		
SET_CELL_SETTINGS	@'43'8,'ARGs(8)'e	@'43'8,'ARGs(8)'e	n.a.		
ASK_MAX_SETTINGS	@'44'0e	@'44'1,'ARG'e	n.a.		
ASK_BMS_SETTINGS	@'45'0e	@'45'2,'ARG'e	n.a.		
ASK_PACK_AMPHOURS	@'46'0e	@'46'1,'ARG'e	Ah		
ASK_PACK_SOC	@'47'0e	@'47'1,'ARG'e	%		

Table 3.3: OBDII commands implemented on ISR-BMS.

Long Name	Short Name	Mode & PID	Equation	Minimum	Maximum	Unit	OBD2 Header
Cell Voltage #1	Cell1	22F100	$((A*256)+B)$	1000	4096	mV	7DF
Cell Voltage #2	Cell2	22F100	$((C*256)+D)$	1000	4096	mV	7DF
Cell Voltage #3	Cell3	22F101	$((A*256)+B)$	1000	4096	mV	7DF
Cell Voltage #4	Cell4	22F101	$((C*256)+D)$	1000	4096	mV	7DF
Cell Voltage #5	Cell5	22F102	$((A*256)+B)$	1000	4096	mV	7DF
Cell Voltage #6	Cell6	22F102	$((C*256)+D)$	1000	4096	mV	7DF
Cell Voltage #7	Cell7	22F103	$((A*256)+B)$	1000	4096	mV	7DF
Cell Voltage #8	Cell8	22F103	$((C*256)+D)$	1000	4096	mV	7DF
Cell Voltage #9	Cell9	22F104	$((A*256)+B)$	1000	4096	mV	7DF
Cell Voltage #10	Cell10	22F104	$((C*256)+D)$	1000	4096	mV	7DF
Cell Voltage #11	Cell11	22F105	$((A*256)+B)$	1000	4096	mV	7DF
Cell Voltage #12	Cell12	22F105	$((C*256)+D)$	1000	4096	mV	7DF
Cell Voltage #13	Cell13	22F106	$((A*256)+B)$	1000	4096	mV	7DF
Cell Voltage #14	Cell14	22F106	$((C*256)+D)$	1000	4096	mV	7DF
Cell Voltage #15	Cell15	22F107	$((A*256)+B)$	1000	4096	mV	7DF
Cell Voltage #16	Cell16	22F107	$((C*256)+D)$	1000	4096	mV	7DF
BMS Temperature	T_Bms	22F0FF	$((A*256)+B)/10$	-10	50	C	7DF
Cells Temperature	T_cells	22F0FF	$((C*256)+D)/10$	-10	50	C	7DF
Pack Current	I_Pack	22F015	$((A*256)+B)/100$	-300	300	A	7DF

Remarks:
 CAN-OBDII Protocol - Always 8 bytes are sent
 nbytes = NewMessageData[0];
 mode = NewMessageData[1];
 pid1 = NewMessageData[2];
 pid2 = NewMessageData[3];
 data=NewMessageData[4-8]
 Standard 11-bits ID
 Message ID 7DF

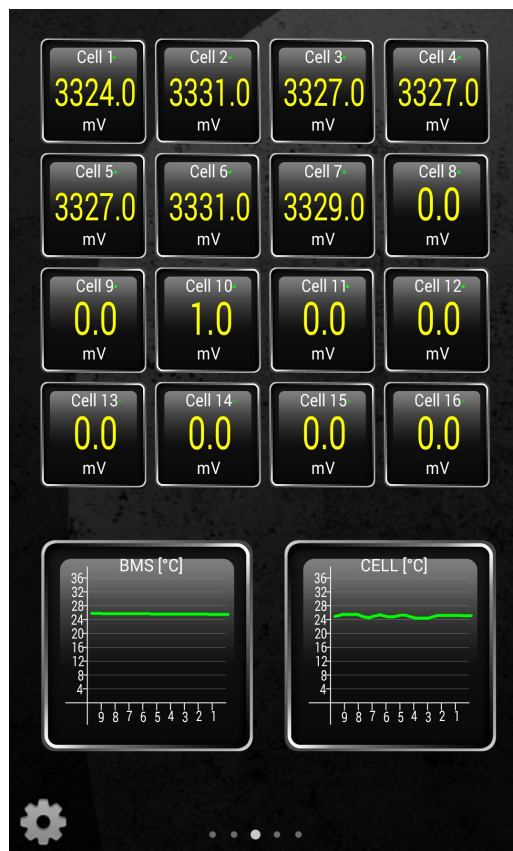


Figure 3.17: Smartphone display of ISR-BMS voltages and temperatures.

3.3.3 The BMS Graphical User Interface for PC

The BMS developed was designed to be flexible. It can be used with different types of Lithium-Ion cells. The MAX14921 can operate with cells voltages in the range of 0.5V to 4.5V and a minimum of 3 Cells. Nevertheless the reference voltage of the ADC will limit the maximum operating voltage of the ISR-BMS to 4.096V. Still the BMS is fully configurable from 3 to 16 cells per module (one master and one slave) and from 0.5 to 4.096V per cell .

It allows for real time cell voltages, current and temperature plotting and data logging to a computer file. Also the cell balancing settings like the start balancing voltage or the allowed delta voltage (the difference between the highest and the lowest cell voltages), can be configured via this interface.

When multiple current sensors or temperature sensors are implemented on the BMS firmware they can also be easily selected from the appropriated combo boxes in the GUI.

The application automatically detects the connection to the BMS and configures the port settings for communication, when a standard USB cable is used to connect the PC with the BMS. An HEARTBEAT command is sent every 0,5s to the PC and is used to toggle an LED that gives a visual feedback of good communication link between the PC and the BMS.

A screenshot of the configuration screen is shown in Figure 3.18 and another one from real time cell voltage plotting in Figure 3.19.

The GUI is documented at Appendix C.

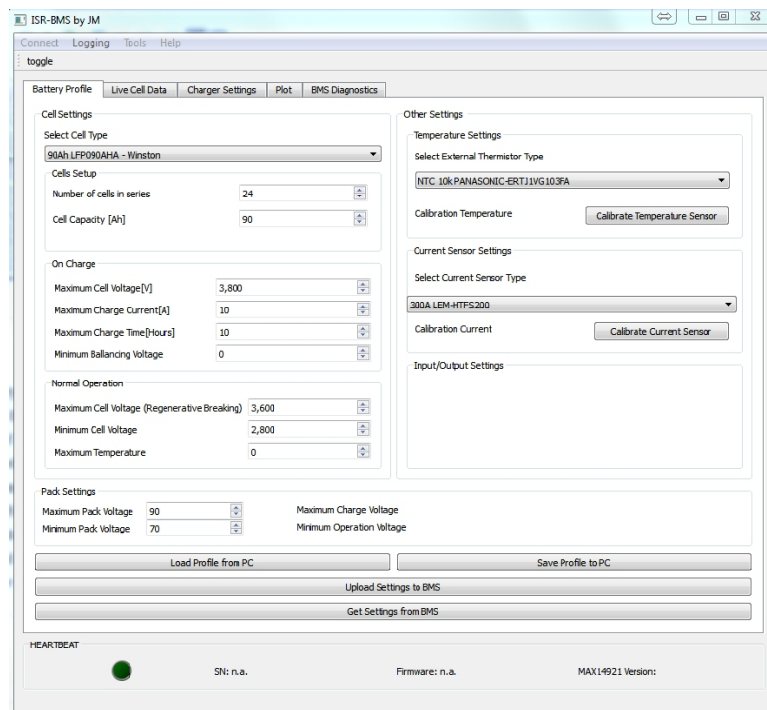


Figure 3.18: ISR-BMS GUI parametrization menu.

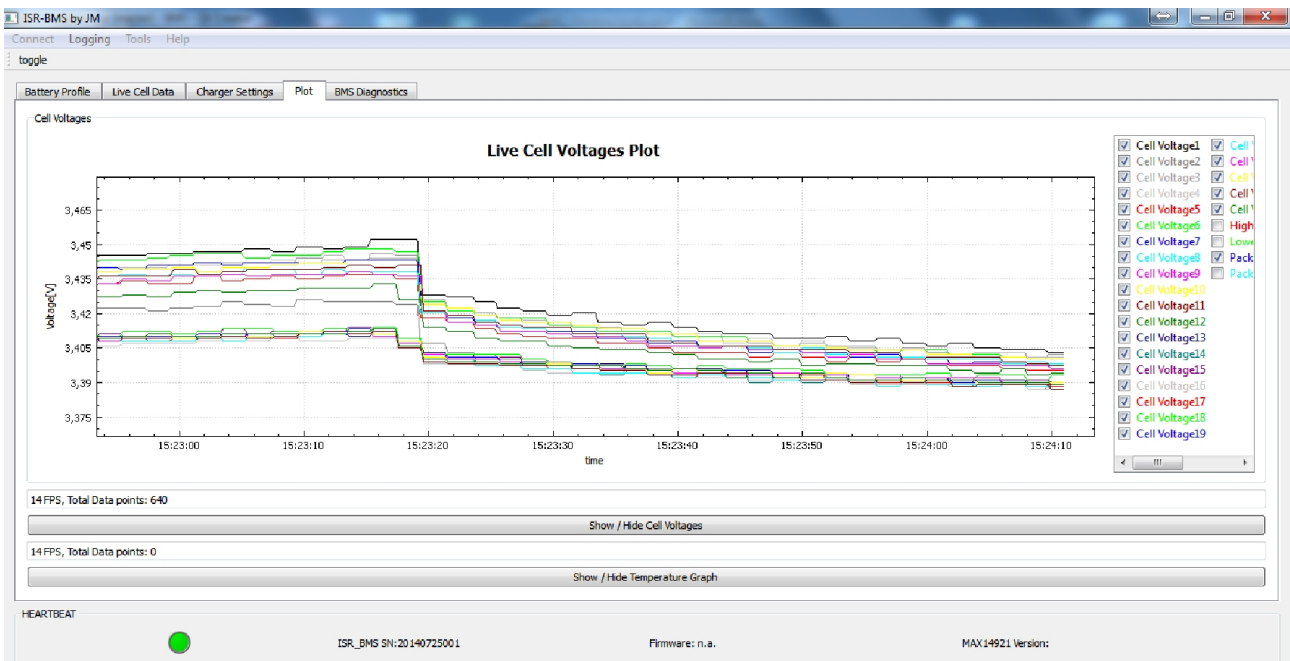


Figure 3.19: ISR-BMS GUI live cell voltages plot.

Chapter 4

Battery Modeling

Users of EVs require precise and reliable information on their autonomy. This information is of paramount importance to avoid range anxiety symptoms.

The SOC of the battery pack on an EV is comparable with the fuel gauge of an internal combustion vehicle. The range estimation algorithms used are only as accurate as the data provided by the BMS about the SOC of the battery pack. The SOC can not be measured directly from the battery terminals. Therefore it needs to be estimated based on the measurable battery parameters (individual cell voltages, current and temperature). This estimation is important not only for optimal battery energy management but also to avoid an overcharge or overdischarge scenario that can represent safety concerns or reduce battery life span. A reliable and precise estimation of the remaining charge available allows the use of the battery full capacity.

An accurate model representing the characteristics of the battery is essential for SOC estimation accuracy. As covered on the State-of-the-Art chapter, battery models range from complex models that reproduce the electrochemical reactions inside the battery, requiring a very high computational effort, to simple models like the coulomb counting that have very good run-time performance but can be very imprecise due to error accumulation from current measurements.

Due to the chosen architecture of the ISR-BMS, the choice of the model is conditioned to the resources available mainly due to the RAM and ROM limitations. Therefore an offline technique to model the cell was used, based on datasets made in Laboratory. The chosen model is an Electrical Equivalent Circuit (EEC) [Huria et al., 2010]. For this purpose an automated test setup was used, that allows to characterize the cell under different charge and discharge conditions at controlled temperature. This test setup is briefly described at the end of this chapter.

4.1 Modeling Method

The EEC models are a good trade-off between complexity and run-time performance and allow to model certain important dynamics of the battery cells. Another important advantage of those models is their ability to calculate both the terminal voltage and cell SOC. This model can also be used in combination with coulomb counting to periodic calibration during rest, based on the OCV/SOC derived correlation. By comparing the model terminal voltage and the

Table 4.1: Overview of Applicable International Standards for Lithium-Ion cells or batteries

Standard	Title
ISO 12405-1	Electrically propelled road vehicles–Test specification for lithium-ion traction battery packs and systems–Part 1: High-power applications
ISO 12405-2	Electrically propelled road vehicles–Test specification for lithium-ion traction battery packs and systems–Part 2: High-energy applications
IEC 62660-1	Secondary lithium-ion cells for the propulsion of electric road vehicles Part 1: Performance testing
IEC 62660-2	Secondary lithium-ion cells for the propulsion of electric road vehicles Part 2: Reliability and abuse testing

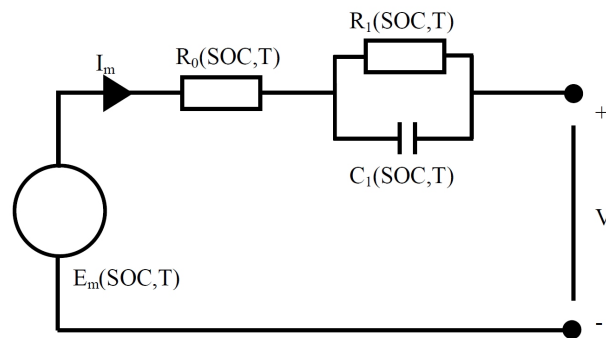


Figure 4.1: EEC model adopted for ISR-BMS

measured cell voltage the model error can be estimated. If enough data logging is provided and computational resources are available, adaptive algorithms such as Extended Kalman Filter (EKF) [Plett, 2004] can be used to improve the SOC accuracy.

The employed modeling method follows the applicable standards for Lithium-Ion cells and battery packs whenever the bench test setup allows. The present test setup is limited to temperatures between 0 and 45°C, charge currents up to 30A and discharge currents up to 20A. So the tests that require negative temperatures or higher charge or discharge rates can not be performed with the present test setup. The relevant standards are summarized on Table 4.1.

Most models in the literature do not consider the thermal effects. It was adopted the model presented by [Huria et al., 2010] that tackles this limitation by including the temperature as an independent variable in the look-up tables that define the circuit elements.

The adopted model is represented in Figure 4.1.

This model, despite its simplicity can fit experimental data reasonably well for the tested

conditions. It is also suitable for embedded applications like the presented one. Of course it can not model the different dynamics of a battery as it is limited by the use of a single RC branch, so a single time constant.

The choice of this model requires the estimation of four independent parameters, namely the electromotive force (E_m), the series resistance (R_o), and the parallel RC branch (R_1, C_1), which in turn, vary with the temperature and the SOC of the cell.

The SOC of a cell is typically presented as the remaining charge available on the cell. It is function of the full cell capacity C_Q at the temperature and discharge current considered and the extracted charge Q_e :

$$SOC = 1 - Q_e/C_Q \quad (4.1)$$

Assuming the cell to be fully charged at time $t=0$ Q_e can be defined as ,

$$Q_e(t) = \int_0^t I_m(\tau) d\tau \quad (4.2)$$

It is usually given as a percentage of the full cell capacity. This capacity represents the maximum extractable charge under certain conditions and depends on the following factors:

- The charge and discharge rates;
- The temperature;
- The value of the cut-off discharge voltage;
- The age of the cell.

Consequently, any SOC definition should consider the conditions under which a cell is discharged and refer to the particular discharge current and temperature under which the SOC has been evaluated.

4.2 Description of Tests Performed

The cells were preconditioned prior to any measurements for data fitting with the model. The tests were performed on the model LFP090AHA from Winston manufacturer, a prismatic 90Ah of Lithium Iron Yttrium Phosphate (LiFeYPO₄) chemistry.

The cell specifications are shown on Table 4.2.

Table 4.2: LFP090AHA cell specifications.

Model name	LFP090AHA	Older product marking TS-LFP90AHA, TS-LYP90AHA
Nominal voltage	3.2 V	Operating voltage under load is 3.0 V
Capacity	90 AH	+/- 5%
Operating voltage	max 4.0V - min 2.8V	At 80% DOD
Deep discharge voltage	2.5 V	The cells is damaged if voltage drops bellow this level
Maximal charge voltage	4.0 V	The cells is damaged if voltage exceeds this level
Optimal discharge current	< 45 A	0.5 C
Maximal discharge current	< 270 A	3 C, continuous for max 15 minutes from full charge
Max peak discharge current	< 1800 A	20 C, maximal 5 seconds in 1 minute
Optimal charge current	< 45 A	0.5 C
Maximal charge current	< 270 A	< 3 C with battery temperature monitoring
Maximal continuous operating temperature	80 °C	The battery temperature should not increase this level during charge and discharge
Dimensions	143x61x218 mm	Millimeters (tolerance +/- 2 mm)
Weight	3.1 kg	Kilograms (tolerance +/- 150g)

4.2.1 Pre-conditioning

This test is done only with new cells. It consist on some cycles of charge/discharge at room temperature, aiming to reach a stable and replicable status of the cells.

This test is not foreseen on the IEC62660-1 but it is important to reach a stable electrochemical status with a predictable capacity. This procedure is foreseen on the ISO12405 and applies to battery packs and systems.

Procedure:

- The test is performed at room temperature ($25^{\circ}\text{C} \pm 2^{\circ}\text{C}$).
- The discharge is performed at C/3 until the minimum voltage recommended by the supplier is reached.
- The charge is CC up to the maximum charging voltage and CV after that until the charging current reduces to C/10.

The cell is considered “pre-conditioned” when the discharged capacity during two consecutive discharges, does not change by a value greater than 3% of the rated capacity.

Due to the cell characterization setup the charge and discharge currents were reduced to 20A.

The charge and discharge voltage curve is shown in Figure 4.2. The cell was fully charged, starting from its original SOC, and after that a full discharge-charge cycle was applied. The charge cut-off voltage was set to 3.8V and the discharge cut-off voltage to 2.8V.

The cell capacity measured on the first discharge was 99,6Ah and on the second discharge 99,7Ah varying about 0,11% of the rated capacity. As a result the cells are considered pre-conditioned.

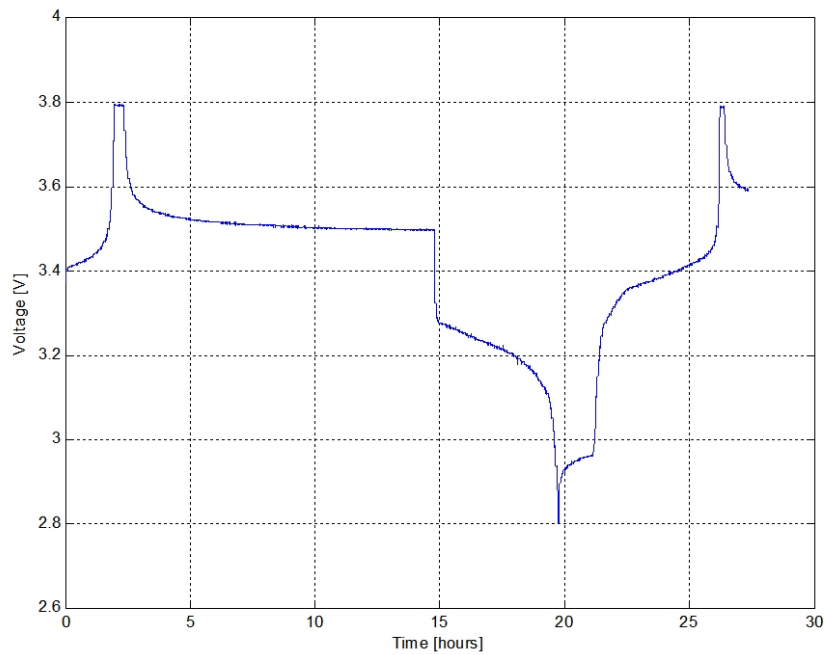


Figure 4.2: Voltage plot of first pre-conditioning cycle.

4.2.2 Characterization Test Setup

To fully characterize the Lithium-Ion cells it is essential to measure their key parameters at different temperatures as their performance is fully dependent on environment conditions.

There are several climatic chambers commercially available but their cost can be prohibitive, are not easy to parametrize or do not have an appropriate interface for being controlled externally.

The required test setup needs as well a controllable DC current load to set the discharge current on the cell and a CC/CV charger to fully characterize the charge/discharge cycle.

To achieve this goal an integrated climate chamber with temperature control and an electronic DC load were designed to be controlled by a microcontroller interfacing with a PC via USB. In this way a rather precise, flexible and affordable setup was achieved.

The cell test setup was developed by a ISR-UC research team, and the author's contribution in the test setup development consisted of the calibration of current measurements, the implementation of remote charge control via PC with local cell voltage sensing and on the GUI implementation (MATLAB) for test setup and data logging via the PC. This setup is shown in Figure 4.3.

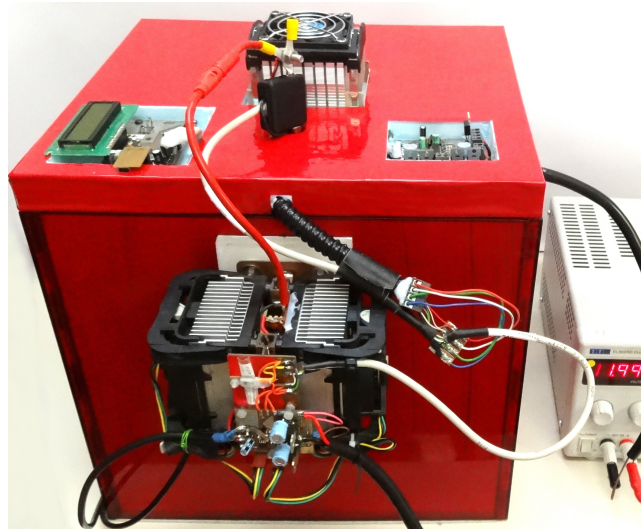


Figure 4.3: Cell characterization test setup.

Its main features are summarized on Table 4.3 .

Table 4.3: Test Setup Features

Measurements	Overall Accuracy
Voltage	0.2%
Current	0.2%
Ambient Temperature	$\pm 0.25^{\circ}\text{C}$
Cell Temperature	$\pm 0.25^{\circ}\text{C}$
Sampling rate	4Hz
Max. Controlled Temperature	45°C
Min. Controlled Temperature	0°C
Max. Discharge Current	20A

The setup is composed by the following elements:

1. The charging system - driven by a 600W DC Power Supply from Delta Elektronika (Model SM1540-D) fully controllable via analog input.
2. The discharge system - a controllable electronic DC load for voltages up to 5V and currents up to 20A.
3. The temperature control system - The temperature is controlled with a 130 W thermo-electric module. For temperature measurements the I2C MCP98908 digital temperature sensor was used. The advantage of this sensor is that it is factory calibrated.
4. The measurement system - The hardware is composed by a microcontroller that interfaces a I2C INA226 (DC accuracy: shunt voltage $2.5\mu\text{V}$, bus voltage 1.25mV, bus voltage range 36V). The setup interfaces with the PC via USB and allows for remote control of temperature, voltage and current, producing charge/discharge profiles.

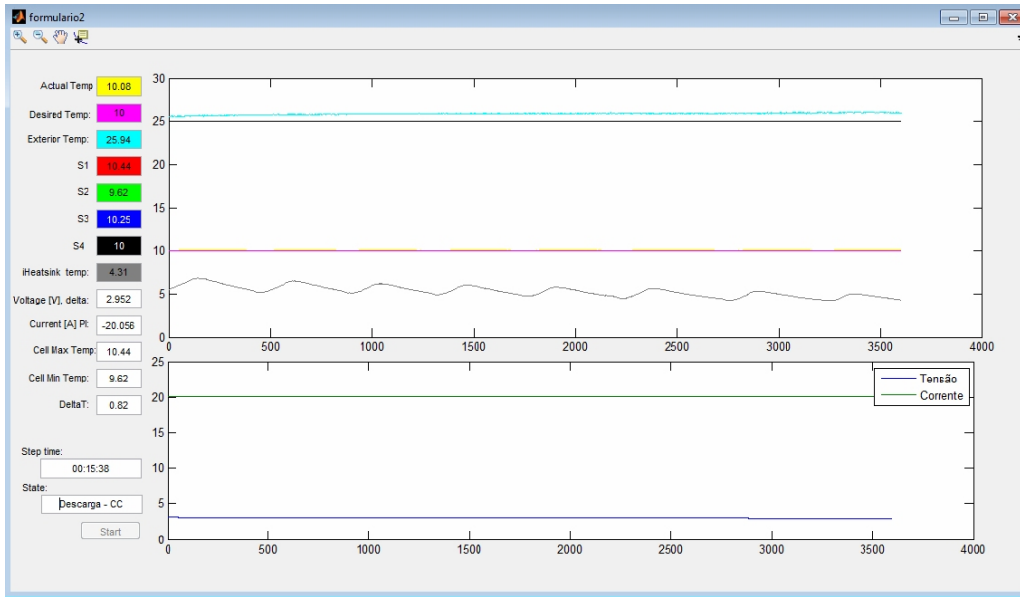


Figure 4.4: Characterization cell box GUI.

A screenshot of the GUI, illustrating the last 10% SOC discharge at 10°C under a constant current of 20A, can be seen in Figure 4.4.

4.2.3 Characterization Tests

The cell under test was discharged in steps of 10% of SOC with a relaxation time of 2 hours within discharges. The SOC was derived based on coulomb counting of the current drawn at each step. The same discharge profile was run at 10, 25 and 45°C.

4.3 Cell Model Derivation

For calculating the model parameters based on available experimental data, the Matlab Simulink GUI estimation tool, developed by Tarun Huria[Huria et al., 2010] was used to obtain the 1 RC branch EEC parameters values lookup tables (10, 25 and 45°C).

This tool also incorporates the cell model created with SimscapeTM blocks and SimscapeTM language allowing for simultaneous simulation of the model.

In Figure 4.5 the output of the estimation and simulation tool can be seen. The fitting looks rather good for a model with a single time constant. The estimated model was able to keep track of the OCV after every discharge pulse.

The experiment at the 3 different temperatures resulted in four sets of data for the 4 elements of the EEC, that characterize the cell chemistry under test. The Figure 4.6 summarizes the obtained data .

Some interesting results can be drawn from the experimental data:

1. The SOC-OCV model curve shows that OCV depends very little from the temperature

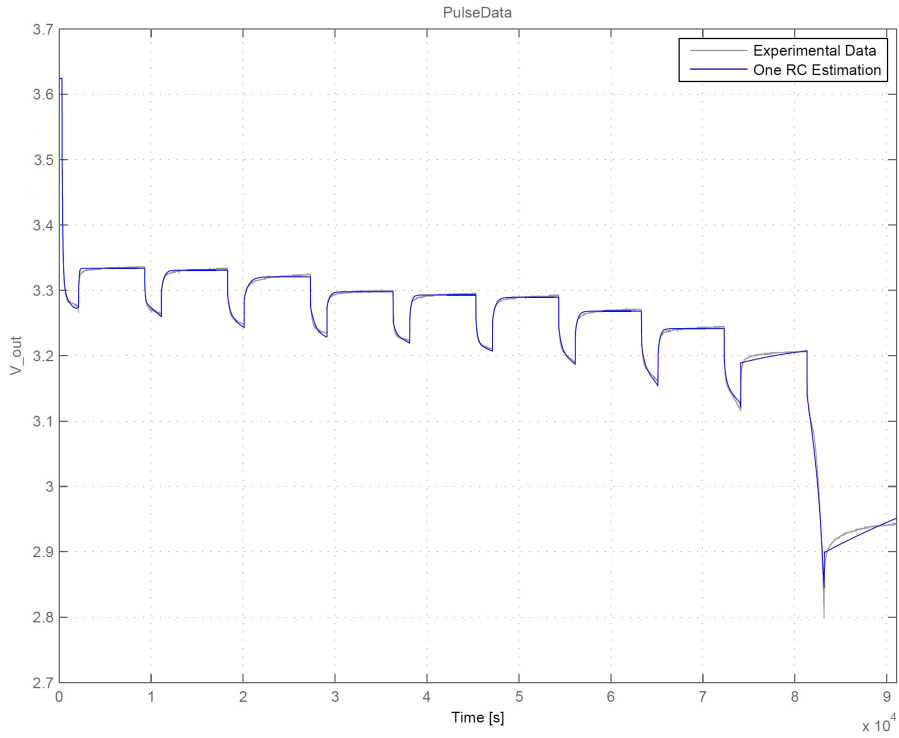


Figure 4.5: Measured versus simulated data at 25 °C.

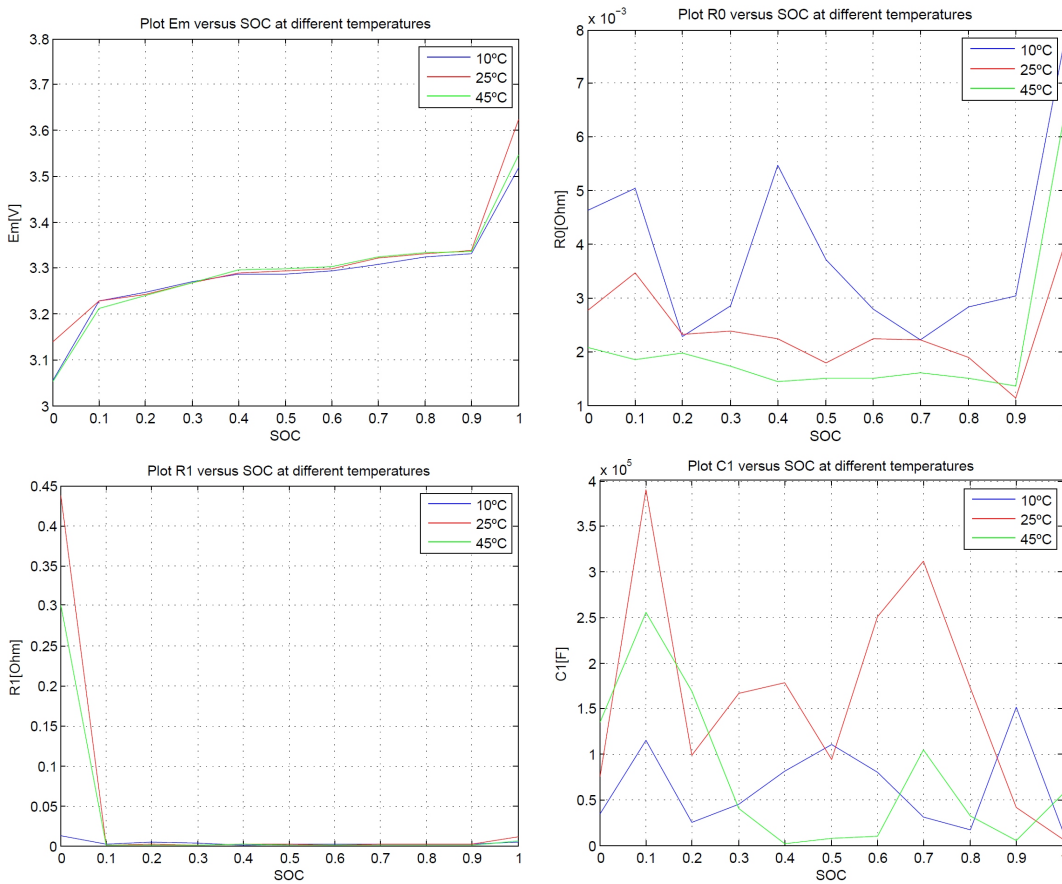


Figure 4.6: EEC estimated parameters.

having a strong dependence on SOC. Also the model shows a less consistent behavior at SOC extremes.

2. R_o shows a dependence on SOC and temperature with a minimum value close to 50% SOC for 25 and 45°C and lower values for higher temperatures. At 10°C it shows an unexpected behavior that could not be confirmed due to the lack of time.
3. R_1 , the resistive component of the RC element, shows little SOC dependence on temperature from 10 to 90%SOC.
4. C_1 , the capacitive element of the RC element does not show a predictable or consistent behavior being difficult to attribute a significance to those values. That is one of the drawbacks of equivalent numerical models compared to physical models that represent the battery internal phenomena.

Chapter 5

BMS Experimental Results

In this Chapter several experimental tests made with the electric platform after the ISR-BMS installation are described. The goal is to validate the measurements taken by the BMS and evaluate its on-line performance as well as its ability to safely charge and balance the battery pack.

5.1 Battery Pack Current Measurements

To validate the current measurements of the ISR-BMS, a simultaneous data log of the BMS readings and a commercial current probe from Fluke (Model i310s) was performed. The current probe used has a bandwidth of 1 kHz and was used with the selected sensitivity of 10 mA/V featuring an accuracy of $\pm 1\%$ of the reading $\pm 50\text{mA}$. The current probe was connected to a PicoScope (Model 4424) with 20 MHz bandwidth and was sampled at 10 Hz. That corresponds to the internal sample rate of the ISR-BMS. Nevertheless the current log was made by the GUI with a sample rate of 1HZ. The comparative result can be observed in Figure 5.1.

The results shows that the ISR-BMS data logged into the PC was not able to accurately follow all the current peaks. This is due to the fact that the sample rate of 1 Hz is not high enough to display the fast transients on the current. But since the internal sample rate is indeed 10Hz the ISR-BMS “senses indeed” the current shown in red and do all its calculations based on that information. This is very important for instance to compute the current integral (coulomb counting) needed for the SOC estimation.

Further testing needs to be done, increasing the GUI sample rate to have a more representative information of the real currents on the PC. This can be important if this information is needed to implement some kind of adaptive SOC estimation algorithm. If needed the ISR-BMS internal sample rate can also be increased.

5.2 Cell Voltages Measurements

The individual cell voltages from the battery pack were also logged in the PC via the developed software. The result can be seen in Figure 5.2.

This plot shows interesting information. As mentioned before the battery pack is composed by two modules of 12 cells each connected in series. The cells 1 to 12 were used in a previous project and the cells 13 to 24 were new cells acquired to complete the battery pack. The

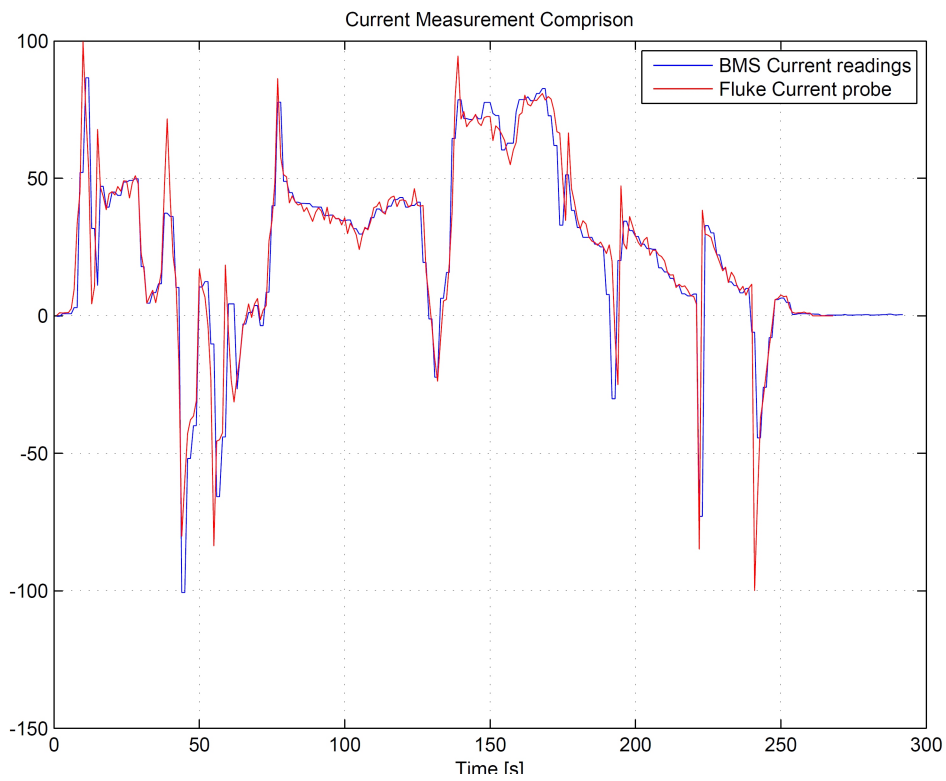


Figure 5.1: Comparative current measurements of ISR-BMS and Fluke i310s current probe.

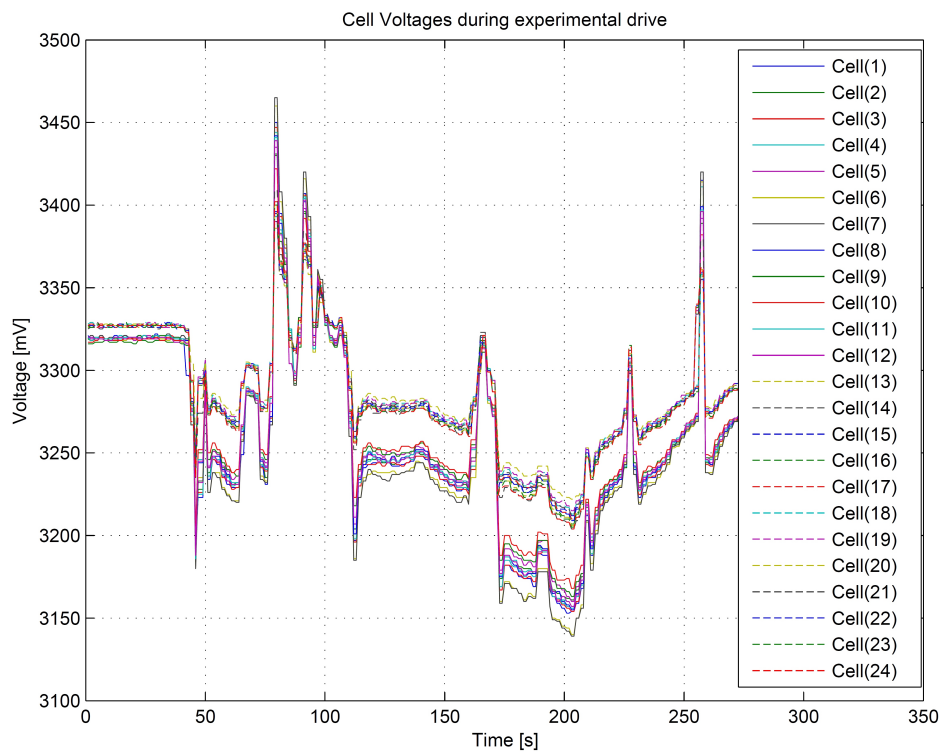


Figure 5.2: Voltage measurements logged on the PC during a real road drive.

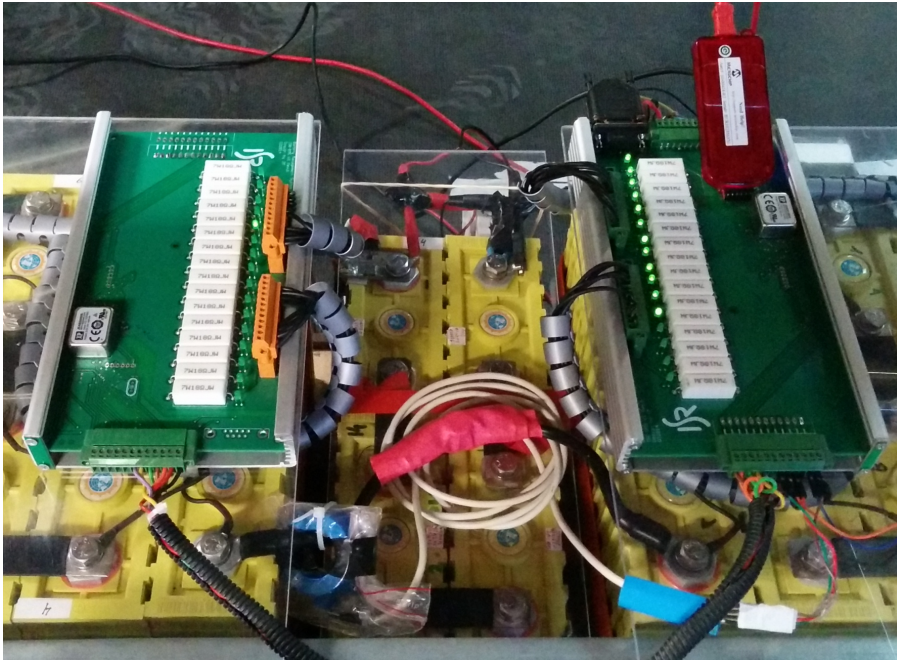


Figure 5.3: BMS debugging after installation.

difference between the two groups of cells is clearly seen on the plot where the used cells show a higher voltage drop during discharge currents due to the increased internal resistance that Lithium-Ion cells face with cycling and aging. It is also possible to see that during the relaxation period or during the regenerative charging the terminal voltages converge to the same value.

This will of course bring some problems to the effective use of the capacity of the new cells since the old cells will have a lower efficiency and need to spend more energy to supply the needed power to the powertrain. So they will reach the end of charge threshold voltage or the 0% SOC before the new cells and no more energy can be drawn from the battery to avoid its overdischarge that could seriously damage the cells.

5.3 Battery Balancing

In this specific case the passive cell balancing is not a perfect solution, as the used cells will reach the start balancing voltage threshold in block and the BMS will turn on the respective balancing resistor leading to a situation where 200mA will be drawn from each cell in order to lower its charge and allow the other block to charge. This represents a dissipation of about 8.5W in the used BMS module that will be dissipated in the form of heat on the balancing resistors that can be seen on the top of the ISR-BMS printed circuit board. This can be seen in Figure 5.3. It is confirmed by the GUI voltages plot in Figure 5.4, where the cells are charging and the terminal voltages of the used cells are reaching the balancing threshold voltage of 3.4 V in block.

The electric platform is equipped with a Robot Operating System (ROS) that allows an



Figure 5.4: Cell voltages during charge at 10A constant current.

easy acquisition and integration of data from different kinds of sensors. The vehicle is already reading the data from GPS, inertial sensors and encoders placed on the wheels. Thanks to João Sousa that created a new ROS node to read the relevant parameters from the BMS it was possible to acquire a combined dataset with information of the ISR-BMS, GPS, and encoders allowing to calculate the car speed and to know its position at each moment. Also the elevation can be computed from the collected GPS data. This combined information can prove very useful to implement range estimation algorithms for people doing research on this field. This combined information is shown in Figure 5.5.

5.3: Battery Balancing

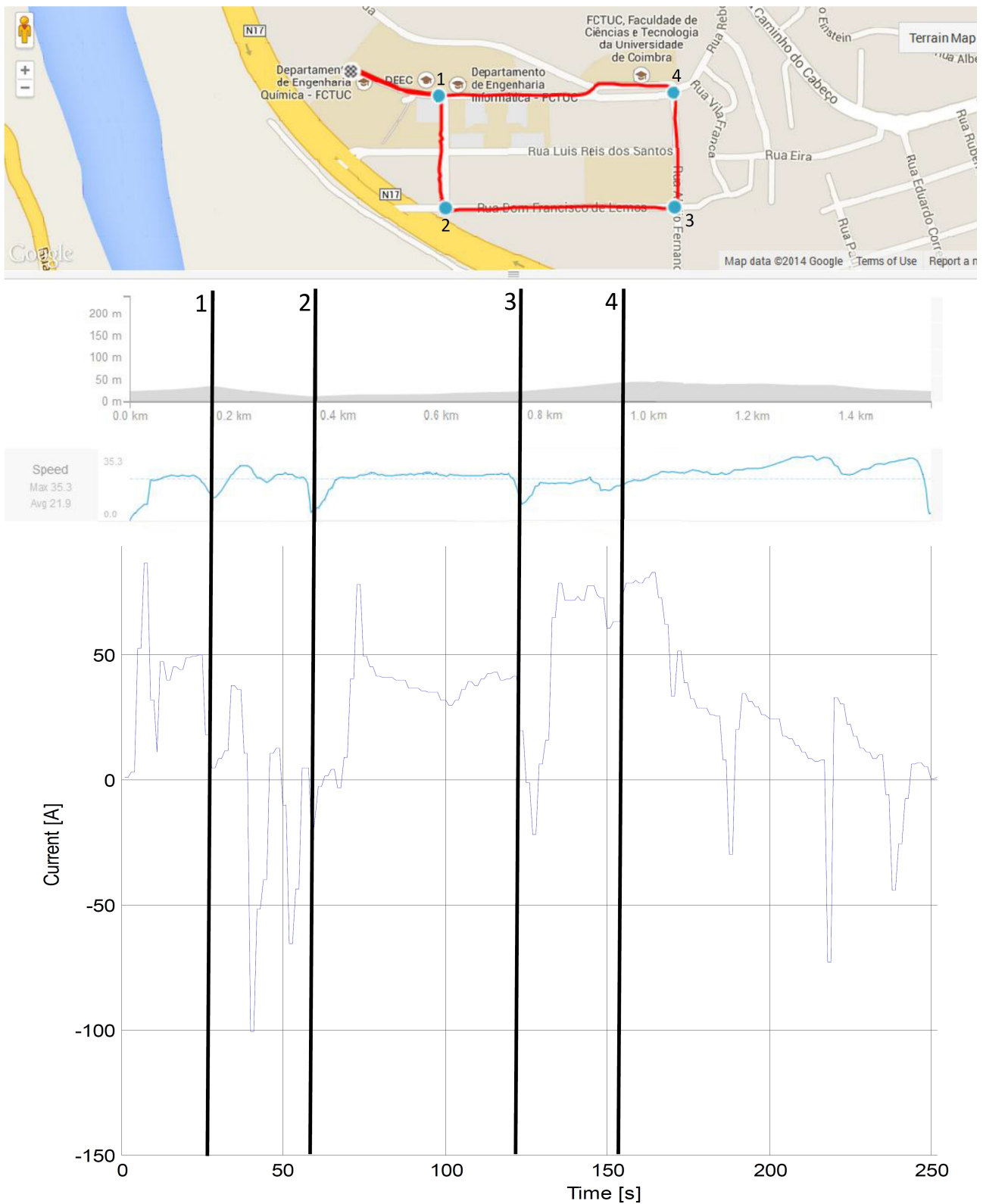


Figure 5.5: Combined information of ISR-BMS, GPS and encoders from the electric platform during a real road drive.

5.4 ISR-BMS Benchmarking

The ISR-BMS was compared with two existing commercial BMSs, namely the ORION BMS from the American company Ewert Energy Systems, Inc and the EMUS BMS from the Lithuanian company Elektromotus. The results are shown on Figure 5.6



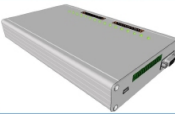
 ORION	 EMUS	 ISR - BMS
Centralized	Distributed	Centralized
1~180	4~256 cells	3~16 Master 6~32 Master/Slave
Any cell shape	Prismatic Cells	Any cell Shape
200mA	Up to 1.3A Balancing Current (Configurable)	Default 200mA Settable by external resistor
CAN OBDII Support	CAN, USB, RS232	CAN, USB OBDII Support
One current Sensor , 4 thermistors (extendable by external module)	One current sensor(optional), one temperature sensor per cell.	One current Sensor, up to 5 thermistors (NTC)
V, I, T, Pack Voltage, SOC, RI, OCV estimation	V,I, Cells Temperatures, SOC	V, I, T, Pack Voltage, SOC, OCV- SOC correction

Figure 5.6: Benchmarking the ISR-BMS with other commercial BMSs.

Chapter 6

Conclusion and future work

6.1 Conclusion

During this dissertation a lot of know-how was built around the Lithium-Ion batteries behavior. A simple EEC model with one RC branch revealed a reasonably good capacity to follow the cell dynamics but with limitations to represent the long time constants of the relaxation periods.

The developed BMS hardware is fully functional and able to perform accurate measurements of individual cell voltages, current and temperature. It can perform passive cell balancing for the whole pack based on individual cell information, allowing this way to reduce the differences on the SOC of the different cells optimizing in this way the useful battery pack capacity. It was designed as well to allow the implementation of different charging, cell balancing algorithms and SOC estimation techniques that are not possible to implement on typical commercial BMSs.

It took a long journey to reach this level of functionality and reliability. During the development process, a lot of unpredictable situations occurred that had to be resolved in order to progress. Problems like noise, ground loops, inconsistent communication within the BMS blocks or between the BMS and the PC, bad contacts that lead to intermittent failures are just a few of a long list. Most of those problems would not be present on simulations. They are inherent problems of hardware without a generic solution. Mixed circuit boards with analog and digital signals also place extra challenges. Some of the problems found, took days or even weeks of intensive debugging to be overcome.

Due to the time limitation, it was not possible to implement and validate the cell model on the ISR-BMS during this dissertation.

Working on a battery pack with a build up voltage of 80V and cells that can deliver hundreds of Ampere during normal operation or even more during short-circuits is a dangerous work. All the measures that can be taken to avoid any (unintentional) occurrence of a partial or total short circuit should be taken.

6.2 Future work

As mentioned before this work will continue. In the short term the derived model should be implemented and validated. This model have of course some limitations, therefore more complex models can be used that can follow the different dynamics of the Lithium-Ion Cells.

Moving from a 1 RC branch to a 2 RC branch will increase the model accuracy but also the complexity of estimating the model parameters and of implementing the model.

The 8-bit hardware architecture can also evolve to a 16-bit microcontroller architecture to accomplish the higher processing power required to implement more complex models or higher sampling rates.

Implementing active cell balancing techniques is also a field to explore.

Bibliography

- [Antaloae et al., 2012] Antaloae, C., Marco, J., and Assadian, F. (2012). A novel method for the parameterization of a li-ion cell model for ev / hev control applications. 61(9):3881–3892.
- [AS8506,] AS8506. Datasheet rev 1.Lithium-Ionbattery cell monitor and balancer IC. Available online:<http://www.ams.com/eng/content/download/476603/1402377/244331>.
- [BCG, 2010] BCG (2010). Batteries for electric cars. *Challenges, Opportunities, and the Outlook to 2020. The Boston Consulting Group.*
- [Bergveld, 2001] Bergveld, H. J. (2001). *Battery Management Systems Design by Modelling.*
- [BQ76PL536,] BQ76PL536. Datasheet rev 1.Lithium-Ion battery monitor and secondary protection IC. Available online:<http://www.ti.com/lit/gpn/bq76pl536>.
- [Cao et al., 2008] Cao, J., Schofield, N., and Emadi, A. (2008). Battery balancing methods: A comprehensive review. *2008 IEEE Vehicle Power and Propulsion Conference*, pages 1–6. Available from: <http://ieeexplore.ieee.org/lpdocs/epic03/wrapper.htm?arnumber=4677669>.
- [CARB, 2007] CARB (2007). Status and prospects for zero emissions vehicle technology. *California Air Resources Board, Report of the ARB independent expert panel.*
- [Chen and Rinc, 2006] Chen, M. and Rinc, G. A. (2006). Accurate electrical battery model capable of predicting runtime and i-v performance. 21(2):504–511.
- [Coleman et al., 2007] Coleman, M., Lee, C. K., Zhu, C., Hurley, W. G., and Soc, A. S.-o.-c. (2007). State-of-charge determination from emf voltage estimation : Using impedance , terminal voltage , and current for lead-acid and lithium-ion batteries. 54(5):2550–2557.
- [Daowd et al., 2011] Daowd, M., Omar, N., Bossche, P. V. D., and Mierlo, J. V. (2011). A Review of Passive and Active Battery Balancing based on MATLAB/Simulink. xx(September).
- [Electronicdesign, 2012] Electronicdesign (2012). Anodes, cathodes, and electrolytes. Available from: <http://electronicdesign.com/power/understanding-factors-lithium-battery-equation>.
- [Electropaedia, a] Electropaedia. Battery protection system. Available from: <http://www.mpoweruk.com/safety.htm>.
- [Electropaedia, b] Electropaedia. Temperature and discharge rate. Available from: <http://www.mpoweruk.com/soc.htm>.

- [Energy, 2012] Energy, E. (2012). Cost and performance of ev batteries. *Final report for The Committee on Climate Change*. Available from: http://www.element-energy.co.uk/wordpress/wp-content/uploads/2012/06/CCC-battery-cost_-Element-Energy-report_March2012_Finalbis.pdf.
- [Faria et al., 2013] Faria, R., Marques, P., Moura, P., Freire, F., Delgado, J., and de Almeida, A. T. (2013). Impact of the electricity mix and use profile in the life-cycle assessment of electric vehicles. *Renewable and Sustainable Energy Reviews*, 24:271–287. Available from: <http://linkinghub.elsevier.com/retrieve/pii/S1364032113002220>.
- [Georges, 2014] Georges, J. (2014). Getting the Most Out of the MAX14920/MAX14921 High-Accuracy Battery-Measurement AFEs.
- [Huet, 1998] Huet, F. (1998). A review of impedance measurements for determination of the state-of-charge or state-of-health of secondary batteries. 70:59–69.
- [Huria et al., 2010] Huria, T., Ceraolo, M., Gazzarri, J., and Jackey, R. (2010). High fidelity electrical model with thermal dependence for characterization and simulation of high power lithium battery cells.
- [Kuhn et al., 2005] Kuhn, B., Pitel, G., and Krein, P. (2005). Electrical Properties and Equalization of Lithium-Ion Cells in Automotive Applications. *2005 IEEE Vehicle Power and Propulsion Conference*, pages 55–59. Available from: <http://ieeexplore.ieee.org/lpdocs/epic03/wrapper.htm?arnumber=1554532>.
- [Maxim, 2014] Maxim (2014). Datasheet rev 1. High-accuracy 12-/16-cell measurement AFEs. Available online: <http://datasheets.maximintegrated.com/en/ds/max14920-max14921.pdf>.
- [Ng et al., 2009] Ng, K. S., Moo, C.-S., Chen, Y.-P., and Hsieh, Y.-C. (2009). Enhanced coulomb counting method for estimating state-of-charge and state-of-health of lithium-ion batteries. *Applied Energy*, 86(9):1506–1511. Available from: <http://linkinghub.elsevier.com/retrieve/pii/S0306261908003061>.
- [ORION, 2014] ORION (2014). Orion bms. Available from: <http://www.orionbms.com>.
- [Parthiban et al., 2007] Parthiban, T., Ravi, R., and Kalaiselvi, N. (2007). Exploration of artificial neural network [ANN] to predict the electrochemical characteristics of lithium-ion cells. *Electrochimica Acta*, 53(4):1877–1882. Available from: <http://linkinghub.elsevier.com/retrieve/pii/S001346860701047X>.
- [Piller et al., 2001] Piller, S., Perrin, M., and Jossen, A. (2001). Methods for state-of-charge determination and their applications. 96:113–120.

- [Plett, 2004] Plett, G. L. (2004). Extended kalman filtering for battery management systems of lipb-based hev battery packs: Part 1. background. *Journal of Power sources*, 134(2):252–261.
- [Rahimi-eichi, 2013] Rahimi-eichi, H. (2013). Battery management system - an overview of its application in the smart grid and evs. (June):4–16.
- [Rosenkranz et al.,] Rosenkranz, C. A., Liska, J. L., Controls-saft, J., Daney, B. A., and Bordeaux, F. Modern Battery Systems for Plug-In Hybrid Electric Vehicles.
- [Salkind et al., 1999] Salkind, A. J., Fennie, C., Singh, P., Atwater, T., and Reisner, D. E. (1999). Determination of state-of-charge and state-of-health of batteries by fuzzy logic methodology. *Journal of Power Sources*, 80(1-2):293–300. Available from: <http://linkinghub.elsevier.com/retrieve/pii/S0378775399000798>.
- [Schweighofer et al., 2003] Schweighofer, B., Raab, K. M., Brasseur, G., and Member, S. (2003). Modeling of high power automotive batteries by the use of an automated test system. 52(4):1087–1091.
- [Silva et al., 2012] Silva, M., Moita, F., Nunes, U., Garrote, L., Faria, H., and Ruivo, J. (2012). ISRobotCar: The autonomous electric vehicle project. *2012 IEEE/RSJ International Conference on Intelligent Robots and Systems*, pages 4233–4234. Available from: <http://ieeexplore.ieee.org/lpdocs/epic03/wrapper.htm?arnumber=6386292>.
- [Tao et al., 2011] Tao, H., Feng, Z., Liu, H., Kan, X., and Chen, P. (2011). Reality and Future of Rechargeable Lithium Batteries. (1):204–214.
- [Tarascon and Armand, 2001] Tarascon, J. and Armand, M. (2001). Issues and challenges facing rechargeable lithium batteries. *Nature* 414, 359-367.
- [Tie and Tan, 2013] Tie, S. F. and Tan, C. W. (2013). A review of energy sources and energy management system in electric vehicles. *Renewable and Sustainable Energy Reviews*, 20:82–102. Available from: <http://linkinghub.elsevier.com/retrieve/pii/S1364032112006910>.
- [Wikipedia,] Wikipedia. History of the electric vehicle. Available from: http://en.wikipedia.org/wiki/History_of_the_electric_vehicle.
- [Xing et al., 2011] Xing, Y., Ma, E. W. M., Tsui, K. L., and Pecht, M. (2011). Battery management systems in electric and hybrid vehicles. *Energies*, 4(12):1840–1857. Available from: <http://www.mdpi.com/1996-1073/4/11/1840/>.

Appendix

Appendix A

BMS Schematics

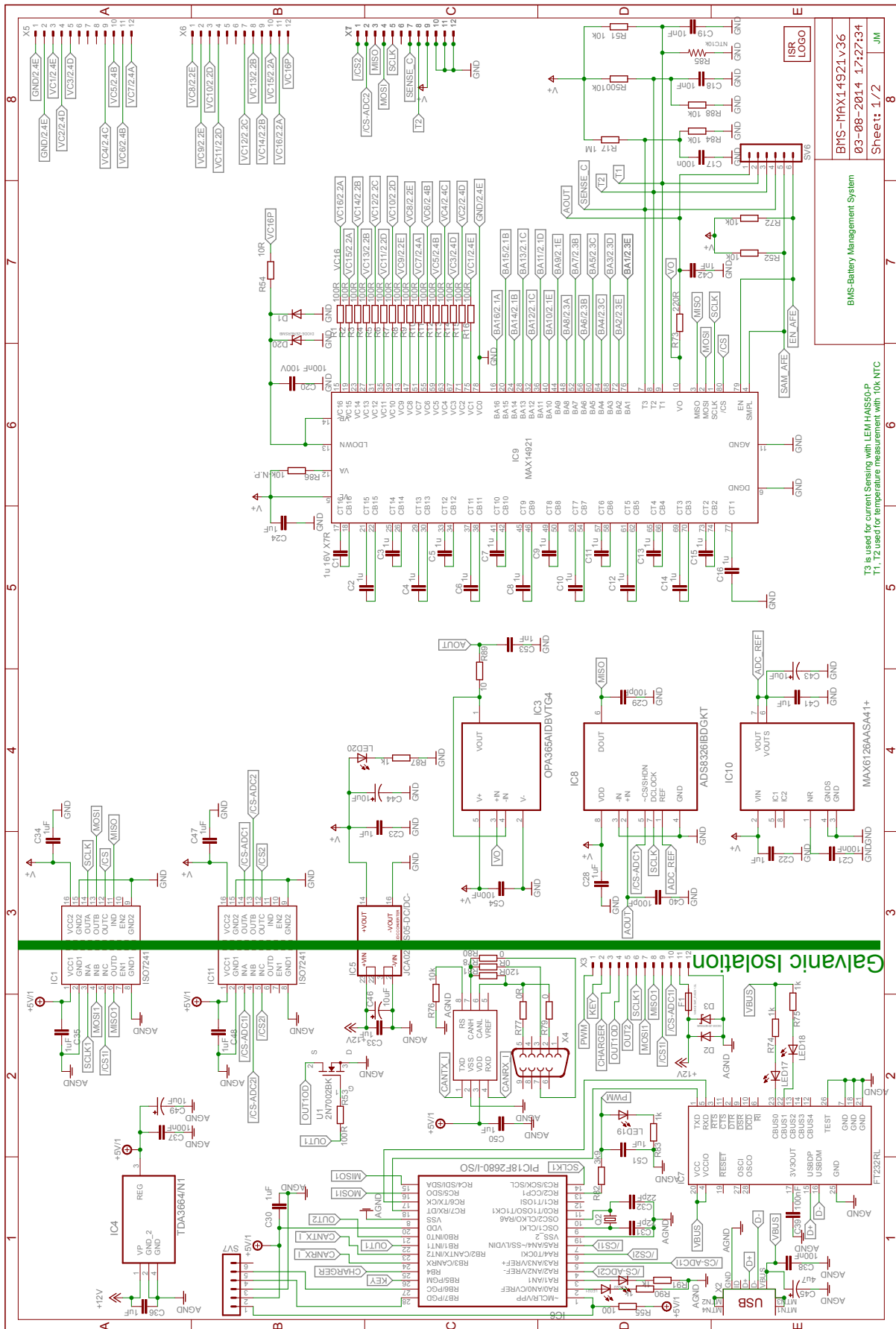


Figure A.1: BMS-ISR Schematics 1/2

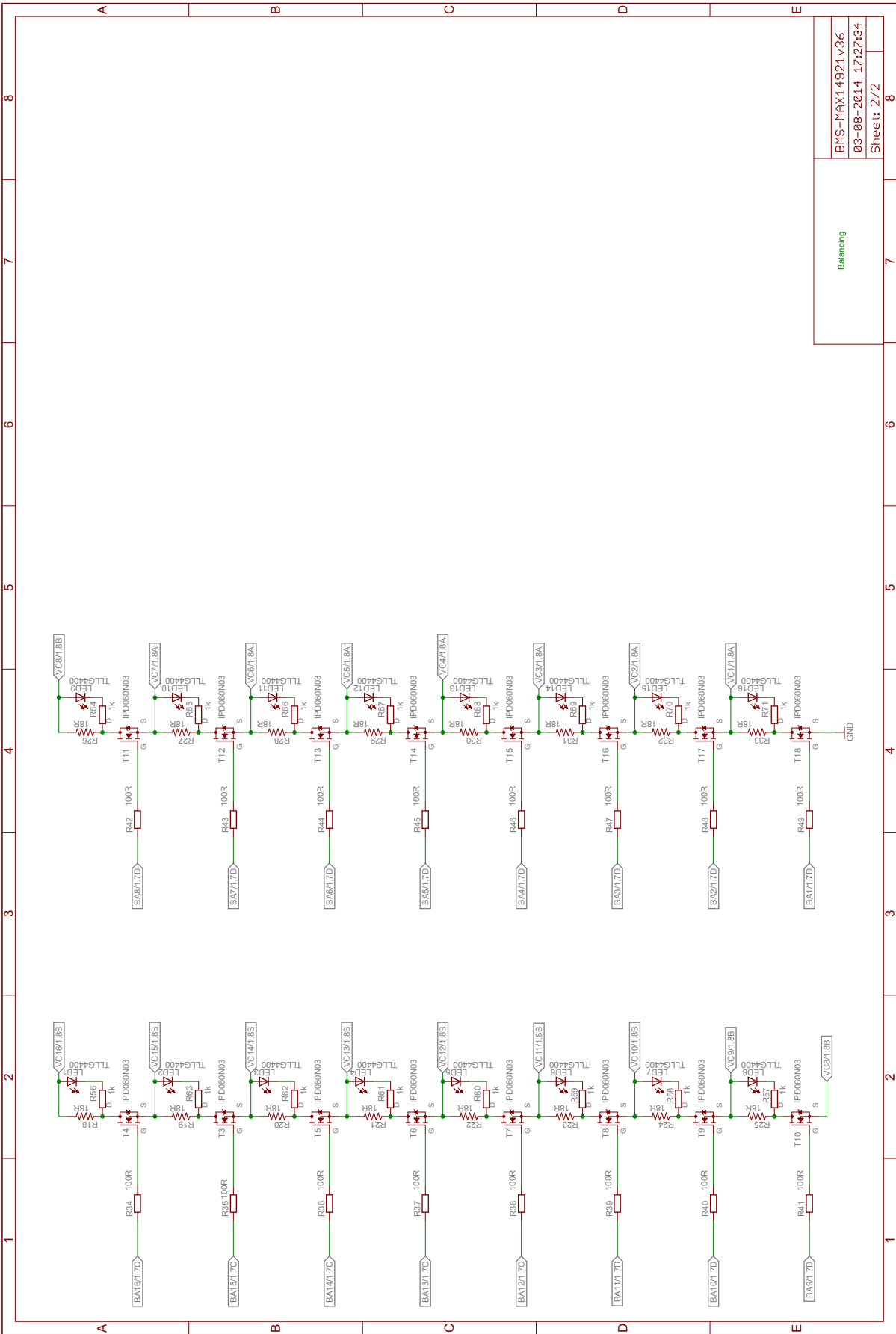


Figure A.2: BMS-ISR Schematics 2/2

Appendix B

Firmware File Structure

File List	
Here is a list of all documented files with brief descriptions:	
[detail level 1 2 3 4 5]	
▼ 00.BMS_firmware	
▼ FreeRTOS	
▼ PIC18_MPLAB	
▼ Headers	
adc.h	Analog to Digital Converter (ADC) functions declaration
afe.h	MAXIM14921 Analog Front End (AFE) functions declaration
CAN18XX8.h	PIC18CXX8 CAN C Library Header File
charger.h	Charger functions declaration
circularbuffer.h	Circular Buffer declaration (implemented for serial port readings)
comcan.h	Communication Routine via CAN - functions declaration and definitions
comserial.h	Communication Routine via Serial Port
FreeRTOSConfig.h	FreeRTOS configuration file
globals.h	Global variables are declared here
inouts.h	Input signals check functions declaration
utilities.h	Delays and other auxiliary functions declaration
▼ Source	
adc.c	Analog to Digital Converter (ADC) functions implementation. Functions are Self Documented
afe.c	MAXIM14921 Analog Front End (AFE) functions and definitions Implementation
charger.c	Charger functions implementation
circularbuffer.c	Circular Buffer implementation(serial port readings)
comcan.c	Communication Routine via CAN - functions declaration and definitions . OBDII support implemented
globals.c	Global variables are set here and declared on globals.h
inouts.c	Input signals check functions declaration
main1.c	Main File with Threads declaration and FreeRTOS initialization routines
utilities.c	Delays and other auxiliary functions implementation


Generated on Sun Aug 31 2014 12:34:51 for BMS Firmware by  1.8.7

Figure B.1: Firmware file structure (by Doxygen)

Appendix C

BMS-ISR Graphical User Interface (GUI)

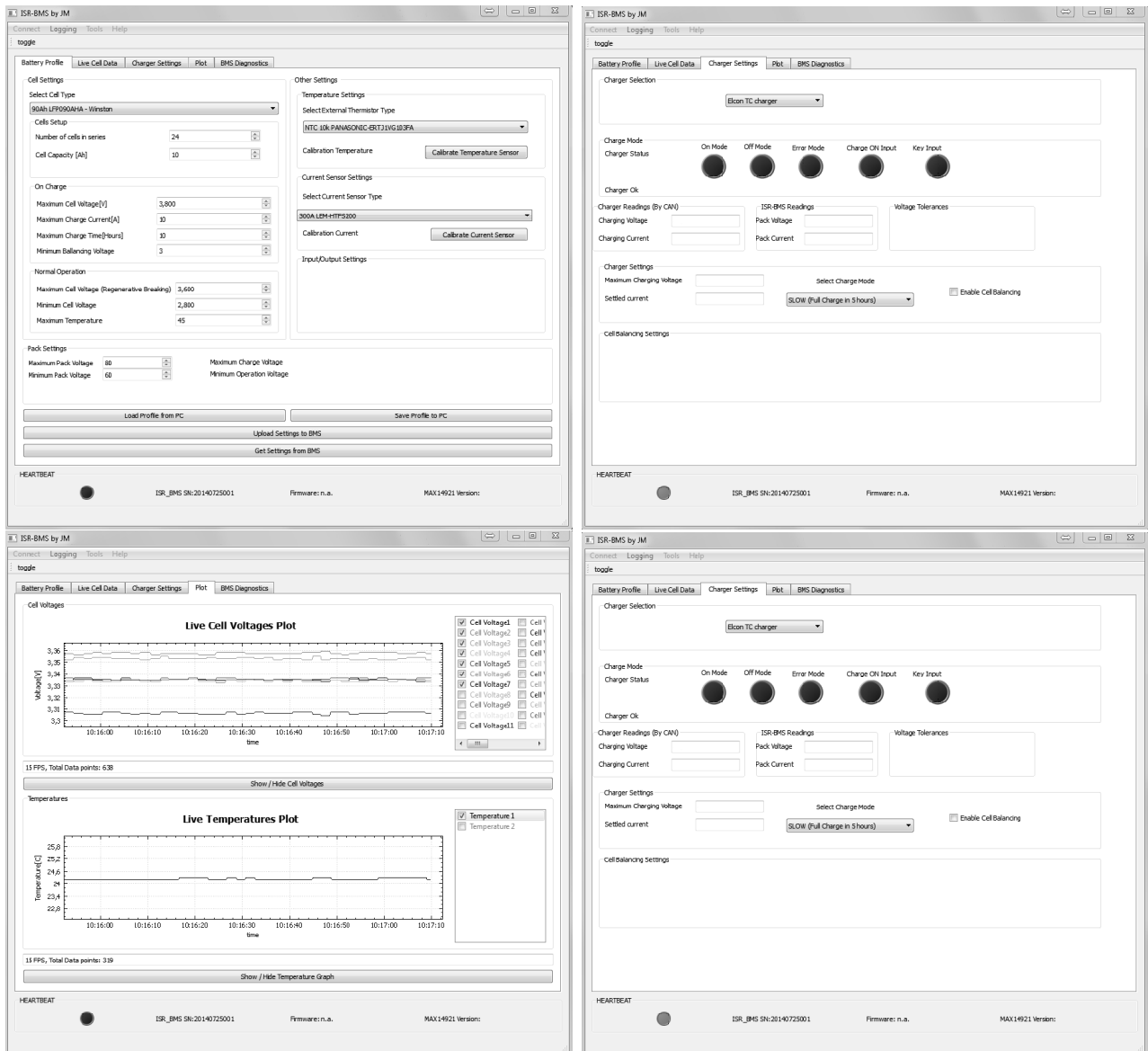


Figure C.1: ISR-BMS GUI.

Appendix D

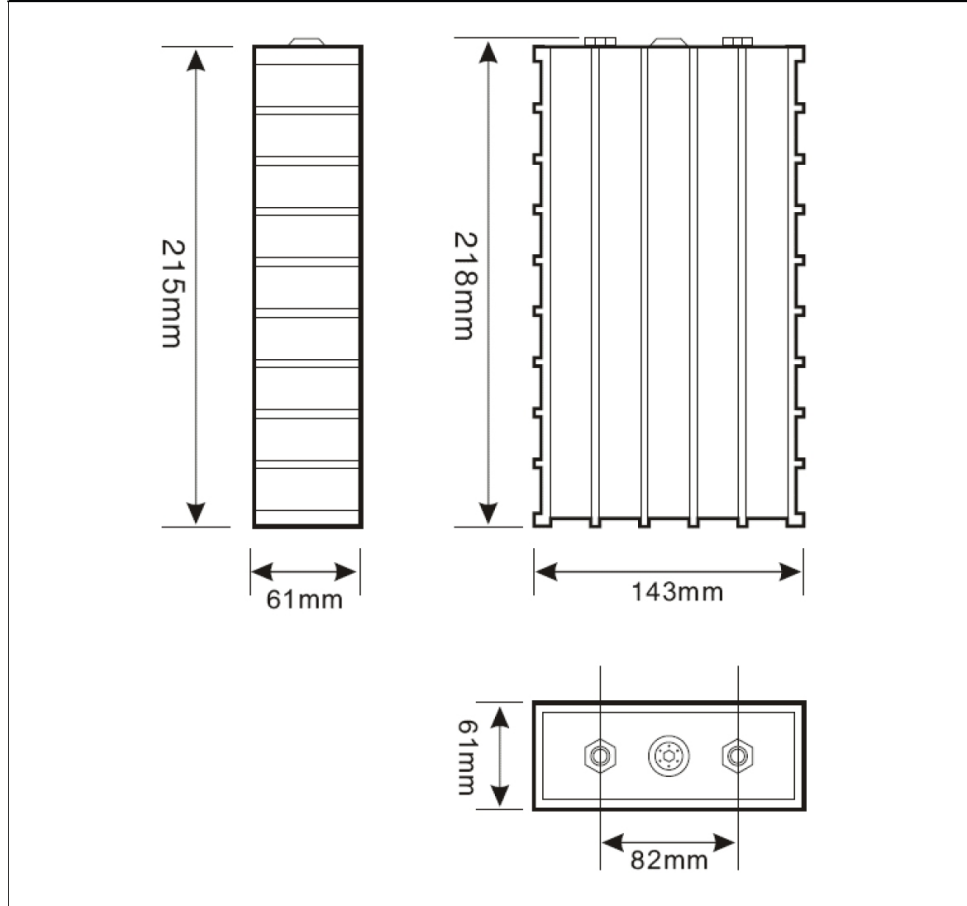
Winston Battery Datasheet

GWL/ Power Group Technology Solutions - Stay Powered for the Future

LFP090AH – WB-LYP90AHA



Model name	LFP090AHA	Older product marking TS-LFP90AHA, TS-LYP90AHA
Nominal voltage	3.2 V	Operating voltage under load is 3.0 V
Capacity	90 AH	+/- 5%
Operating voltage	max 4.0V - min 2.8V	At 80% DOD
Deep discharge voltage	2.5 V	The cells is damaged if voltage drops below this level
Maximal charge voltage	4.0 V	The cells is damaged if voltage exceeds this level
Optimal discharge current	< 45 A	0.5 C
Maximal discharge current	< 270 A	3 C, continuous for max 15 minutes from full charge
Max peak discharge current	< 1800 A	20 C, maximal 5 seconds in 1 minute
Optimal charge current	< 45 A	0.5 C
Maximal charge current	< 270 A	< 3 C with battery temperature monitoring
Maximal continuous operating temperature	80 °C	The battery temperature should not increase this level during charge and discharge
Dimensions	143x61x218 mm	Millimeters (tolerance +/- 2 mm)
Weight	3.1 kg	Kilograms (tolerance +/- 150g)



<http://www.ev-power.eu/>

Figure D.1: Winston battery LYP90AHA.